Advancing Rock-Type Specific Brittle Hoek-Brown Parameter “s”

by

Roman Nesterov

THESIS SUPERVISOR

Suorineni Fidelis Tawiah

THESIS CO-SUPERVISOR

Amoussou Coffi Adoko

Thesis submitted to the School of Mining and Geosciences of Nazarbayev University in Partial Fulfillment of the Requirements for the Degree of
Master of Science in Mining Engineering

Nazarbayev University
April 2025

ORIGINALITY STATEMENT

I, Roman Nesterov, hereby declare that this submission is my own work and to the best of my knowledge it contains no materials previously published or written by another person, or substantial proportions of material which have been accepted for the award of any other degree or diploma at Nazarbayev University or any other educational institution, except where due acknowledgement is made in the thesis.

Any contribution made to the research by others, with whom I have worked at NU or elsewhere is explicitly acknowledged in the thesis.

I also declare that the intellectual content of this thesis is the product of my own work, except to the extent that assistance from others in the project's design and conception or in style, presentation and linguistic expression is acknowledged.

Signed on April 2025

ABSTRACT

The work analyzes sandstone mechanics through laboratory tests consisting of UCS measurements using strain gauges, acoustic emission measurements, and microscopic observations. The first goal of this study was to classify sandstone types through petrographic analysis, followed by the measurement of their compressive stress responses in order to establish rock-type-specific parameters for the Hoek-Brown failure criterion. The study used ten sandstone samples: five fine-grained sandstones and five coarse-grained sandstones. The objective of the study is to determine the relationship between grain size, matrix type, and the brittle Hoek-Brown constant “s” (i.e., cohesion constant). Macroscopic studies combined with microscopic studies provide important results about the structure of the sample, but require more precise measurements between petrographic characteristics such as grain sizes and the Hook-Brown parameter. Petrographic observation showed thin-grained samples had higher matrix material that likely included clay-rich argillaceous material based on their compact, dull appearance. The fine-grained samples studied display arkosic wacke characteristics as a result of high matrix content and poor sorting and angular grain textures, which on thin sections resemble plagioclase feldspar. The thin-section analysis showed that the two sandstone types possessed poor sorting characteristics and included polymictic grain compositions of quartz and plagioclase feldspar, together with iron oxide cement. The fine-grained sandstones contained grains measuring between 60-150 microns, whereas the coarser sandstones held grains from 100 to 300 microns, accompanied by reduced matrix occurrence. The restricted transport patterns, along with quick deposition of angular to sub-angular grain shapes, probably took place in a setting of alluvial fans.

Results from UCS tests showed noticeable differences between the strength of fine- and coarse-grained sandstones. The UCS values of coarse-grained sandstone (103.7-152.6 MPa) exceed the UCS values of fine-grained sandstone (73.9-124.1 MPa) because of different microstructural elements. The better grain interlocking and stronger grain-to-grain contacts within coarse-grained sandstones improve their load-bearing capability. The distribution of stress becomes less effective in fine-grained sandstones because their matrix material includes clay-rich components, which diminishes overall cohesion. The uniaxial compressive strength decreases because poorly sorted and less angular grains found in fine-grained sandstones lead to early stress-induced crack formation. The failure strain of fine-grained sandstones proved lower based on strain gauge measurements, thus indicating these rocks would fail in a more brittle manner than the coarse-grained rocks. The damage initiation stress values are lower in

the fine-grained samples. Under stress conditions, the material experiences early microcrack formation since it contains higher amounts of matrix and grain bonding because of these factors. The research demonstrates that grain size and matrix content directly affect rock strengths as well as the processes through which they fail. The research studied how to improve the brittle Hoek-Brown failure criterion through proper adjustment of its 's' parameter that represents rock material cohesion attributes. Sample analyses indicate that fine-grained sandstone has *s* average parameter value of 0.142, while coarse-grained sandstone has *s* parameter average value of 0.34. The use of s = 0.11 as a generalized cohesion constant lead to forecasting inaccuracies due to significant deviations from the actual values measured during this study, which indicates the need to calibrate the parameter "s" for the type of rock. The study shows that sandstone exhibits varying mechanical responses according to grain size variation and matrix content. The strength values for fine-grained sandstones remain lower than those of coarse-grained sandstones due to their elevated matrix fraction, along with inferior grain bonding strength. This leads to earlier material deterioration. The advanced Hoek-Brown failure criterion gives geotechnical assessments better reliability, which leads to improved underground excavation planning efficiency and safety.

ACKNOWLEDGMENT

In the conclusion of this paper, I experience profound gratitude. Many individuals and organizations presented priceless support that made this experience deliver personal transformation equaling academic success before my graduation. I wish to express sincere gratitude toward everyone who provided either direct or indirect backing over the entire duration of my research.

I want to show my most profound gratitude to Professor Suorineni Fidelis Tawiah for his role as my supervisor. Thanks to his expert guidance together with his consistent support and useful feedback he made this thesis possible. Professor Suorineni Fidelis Tawiah used his deep knowledge of geomechanics together with his expertise and his love for the field to drive me toward academic excellence within my studies while demonstrating me how to continue researching my subject in greater detail. His door stayed open for important discussions even during the busiest periods of his schedule as his guidance developed both my research work and my understanding of scholar and researcher dedication. His extensive understanding made my research possible through all of the research phases that required multiple trial-and-error attempts.

I am grateful to Pallas Resources for providing the sandstone core samples that enabled this research study because of their generous contribution. The experimental part of my research depended intensely on their support, which made its execution possible. My laboratory testing along with analysis stemmed from the core samples, which provided the base for major findings in this thesis. The company demonstrated its appreciation through financial backing while uniting the academic world and industry operations. The participation enabled my research to gain practical significance and real-life implementation, which means a great deal to me.

This thesis included essential lab work, which presented multiple technical difficulties in specimen preparation following ISRM rules and strain gauge setup and calibration procedures. The lab assistant proved essential during this stage of work. Their expertise combined with both their cool approach and help throughout sample preparation and strain gauge setup as well as data gathering and problem-solving guided a safe and efficient testing process. Their patient instruction regarding both laboratory safety procedures and best practices enabled me to gain independence in working with laboratory equipment.

Thank you all.

TABLE OF CONTENTS

LIST OF FIGURES

LIST OF TABLES

1. INTRODUCTION

The assessment of failure conditions is an important aspect in rock mechanics for underground structures design and stability evaluation. In this context, the Mohr-Coulomb (MC) and Hoek Brown failure criteria are two commonly used failure criteria. Specifically, each of these approaches contributes substantially to understanding and predicting the rock mass behavior during the failure under various loading conditions in underground excavation projects.

The Mohr-Coulomb failure criterion is a basic tool to define the failure conditions under shear stress. It is based on shear and normal stresses on the failure plane in the material. The equation is the representation of the criterion itself:

$$\tau = c + \sigma \tan(\phi) \tag{1.1}$$

where c is the cohesion, σ is the normal stress, ϕ is friction, and τ is the shear stress.

When the Mohr-Coulomb failure criterion is used for isotropic materials, the failure conditions can be described as a functional relationship between principal stresses. This equation also excludes the intermediate principal stress, which, more generally in materials with more complex stress conditions, would make it less suitable for rocks. Since it can handle soils and isotropic materials very well, it is not designed to consider jointing, rock mass heterogeneity.

where c is the cohesion, for isotropic materials, if the Mohr-Coulomb failure criterion is used to describe the failure conditions, a functional relationship can be written for the principal stresses. As will be more generally in more complicated stress conditions for materials, this equation does not consider the intermediate principal stress. It cannot handle jointing and rock mass heterogeneity because it is designed to work very well with soils and isotropic materials.

The Hoek-Brown failure criterion stands distinct from others because it focuses on rock mass characteristics to include specific brittle failure behavior of rocks when under stress. The criterion arose through experimental investigations focused on how rocks respond to jointing and geological heterogeneity in most rock masses. The Hoek-Brown criterion contains multiple material constants that represent rock mass quality and jointing properties, thus making it applicable to realistic real-world rock mechanics situations. It can be equated by the next Equation:

$$\sigma_1' = \sigma_3' + \sigma_{ci}\left(m\frac{\sigma_3'}{\sigma_{ci}} + s\right)^{0.5} \tag{1. 2}$$

where σ_1' and σ_3' are the major and minor principal effective stresses, respectively, and σ_{ci} is the uniaxial compressive strength of the intact rock. The parameters *m* and *s* are material constants that depend on the type and condition of the rock mass. The Hoek-Brown criterion accounts for the fact that jointed or disturbed rock masses exhibit lower shear strength compared to intact rock, making it a more accurate tool for evaluating the stability of underground structures in rock.

Multiple modifications have been applied to the Hoek-Brown failure criterion because it needed to account for how rock masses react under different conditions. These modifications enabled the criterion to consider weak rock masses together with disturbed zones as well as additional factors that affect rock behavior in situ conditions.

The material constant named *s* plays the most important role within all parameters in the Hoek-Brown failure criterion. The cohesive strength of the rock mass closely determines this parameter, which plays a major role in stress-related rock mass strength calculations. A standard value of 1 was used for s across all intact rock masses initially, yet this basic assumption did not account for natural rock strength differences between geological settings. According to Hoek et al. from their 2002 publication, the value of s requires modification depending on the rock mass quality. The authors introduced an adjusted relationship by using GSI values for s calculation where GSI represents parameters defining rock mass condition and strength.

$$s = exp(\frac{GSI-100}{9-3D}) \tag{1. 3}$$

where GSI is the Geological Strength Index, and D is a disturbance factor that accounts for the effects of stress relaxation and other forms of damage that may affect the rock mass. This formula allows for a more accurate representation of the rock mass strength by incorporating geological and disturbance factors into the calculation of s.

Using s as a variable according to rock mass quality created better predictions of rock behaviors inside underground spaces. The process of establishing s values for particular rock types continues as a research priority because different geological environments produce diverse rock mass conditions.

The Hoek-Brown criterion adjusts its performance through the m parameter that describes the frictional strength characterizing the mineral mass. Research conducted at Atomic Energy Commission Ltd. (AECL) Underground Research Laboratory in Pinawa by Martin (1993) demonstrated that the frictional strength component m of the Hoek-Brown criterion has a small impact on stress-induced damage of large rock masses. The m value in rock mass analysis becomes negligible when the Geological Strength Index of the rock mass exceeds 65. It is observed that the failure of these rock masses occurs due to the breakdown of cohesion rather than frictional contact. The 'm zero', or 'brittle' Hoek Brown failure criterion was created after setting m equal to zero.

$$\sigma_1 - \sigma_3 = \frac{1}{3} * \sigma_c \tag{1.4}$$

The rock material is defined by the uniaxial compressive strength σ_c.

According to the "m-zero" criterion, every massive rock mass with high GSI values will automatically receive an identical s value of 0.11, although this leads to issues with geological understanding. The assumption fails to appreciate how different rock types respond differently to stress because they do not have identical behavior patterns.

To address these limitations, Suorineni et al. (2009) proposed a modified form of the Hoek-Brown criterion that allows for the use of a constant *A* (constant depending on rock type) instead of a fixed s value. Their revised equation is:

$$\sigma_1 - \sigma_3 = A * \sigma_c \tag{1.5}$$

Suorineni et al. (2009) established a new methodology to determine rock-specific s values through combing laboratory tests and geological field studies. By explicitly considering rock-type characteristics, this method presents a better method to depict the actual behavior of rock masses during tunnel stability evaluations. The research aims to extend the database containing rock-type-specific s values through laboratory investigations of mines located in Kazakhstan. The research for better rock-type awareness of parameter s changes will lead to more precise tunnel stability calculations and increased underground project safety. The Hoek-Brown failure criterion serves as an essential element of rock mechanics when designing tunnels and mines, together with other underground facilities. Further development of material constants continues to be necessary to refine the applicability of the criterion across different rock conditions, particularly the parameters that determine rock mass cohesion strength. The goal of this study is to improve precision in the Hoek-Brown criterion through enhanced knowledge about s values for different rock types, which would result in enhanced tunnel stability evaluations.

1.1 Background/Problem Definition

Conventional tunnel design methodologies often utilize a standardized approach, neglecting the unique characteristics of different rock formations. This can lead to underestimation of potential risks in weaker rock masses and over-engineering in stronger ones. The H-B criteria, while valuable, inherits this limitation. While it provides a framework for rock mass strength estimation, its current form employs a one-size-fits-all approach by relying on two primary parameters: the material constant (mi) and the uniaxial compressive strength (σ_c) [Hoek et al., 2002]. This approach fails to account for the distinct mechanical behaviors exhibited by different rock types due to variations in texture, mineralogical composition, and microstructure. Consequently, the predicted failure depths and required support systems may not be fully optimized for the specific rock mass encountered during excavation.

1.2 Objectives of the Thesis

1.2.1 Main Objectives

The main goal of this research involves the determination of the brittle Hoek-Brown "s" parameter for Sandstones to contribute to the rock-type-specific brittle Hoek-Brown parameters. The research comprises three sequential stages: rock sample laboratory tests and UCS measurements to determine failure onsets. Moreover, this work investigates both ground conditions and geological factors that influence rock brittleness and damage initiation stress.

1.2.2 Specific Objectives

The research specific objective is to fully evaluate a sandstone specimen by using macroscopic and microscopic and mechanical examination methods. The preliminary hand sample classification requires textural and compositional properties identification through the description of grain size distribution and color and matrix content analysis. Thin-section microscopy analysis provides results that reveal the mineralogical composition and grain size distribution patterns, and textural maturity, as well as sorting characteristics.

The evaluation of sandstone mechanical behavior depends on UIS tests that measure uniaxial compressive strength. The UCS values function as indicators to assess strength moderation according to the classification of poorly sorted, matrix-rich sandstones. Analysis of the strength variations caused by cementation type and grain size, and mineral content helps determine the mechanical stability of the rock. A few critical aspects of experimental work are unified to improve the rock's classification and geological history learning and to validate the rock's safety and influence on subsurface infrastructure and reservoir features.

1.3 Scope of Work

The first part of this thesis concentrates on mechanisms of damage initiation in specific rock types at stress levels where the damage first occurs. The proposed method for accomplishing this goal is the implementation of instrumented UCS testing. The quantity of tests conducted may be limited by the time constant. The deployment of equipment, together with the procurement of consumables, may influence the available time.

2. LITERATURE REVIEW

2.1 Influence of Rock Type Variability on Failure Criteria Modification

The research depends on various rock types demonstrating contrasting mechanical properties regarding strength behavior, failure procedures, and deformation characteristics. Engineering projects using Hoek-Brown failure criteria need calibrated "s" parameters since the accuracy of tunnel stability analysis becomes crucial for different rock types. The assessment takes multiple rock samples through testing to demonstrate the effectiveness of adjusted failure criteria for different geological conditions, strengthening predictive models. The study examines various rock categories that contain these particular groups:

Igneous Rocks (e.g., Granite, Basalt) Typically robust and brittle, prevalent in tunnel excavation.

The metamorphic rocks as a rock group include gneiss, schist marble, and many other formations that have specific failure patterns affected by their directional properties and weaknesses.

The stability of tunnels exhibits distinct characteristics across different sedimentary rock divisions of sandstone, limestone shale because these rock types possess different levels of weakness as well as fracturing behavior. Different mechanical properties found in these rock types expand research opportunities for studying failure criteria alterations more accurately.

2.2 "s" parameter Advancing and Limitations

The stability of the tunnel in excavation governs safe and effective subterranean building projects. An extensive behavior of the rock mass surrounding the structure needs to be evaluated. According to Hoek et al. (2002), the Hoek-Brown failure criteria are well-known for predicting the behavior of rock masses and the probable events of collapse. Among the many parameters that the Hoek-Brown parameter "s" depends on, it is one of the key factors determining the rock mass strength and brittle behavior of this criteria, as shown by Martin et al. (1999). Yet, the conventional method often provides ‘s’ a ‘1’ for all ‘kinds’ of rock, which leads to inaccuracy of the estimated stability (Suorineni et al., 2009). This review of the literature focuses on three main study topics that are used to further the development of intrinsic values "s" distinctive to a given kind of rocks for tunnel stability assessment: limitations of the traditional "s" parameter, methods of distinguishing distinguishing kinds of rock mass products which influence "s," and how great importance it has for picking up the correct "s" evaluation.

A major problem exists with the traditional practice of setting the Hoek-Brown parameter "s" at a constant "1". The evaluation of tunnel failure depths in rock masses demands an accurate "brittle" parameter "s" according to the methodology presented by Martin et al. (1999). The present frictional parameters within the Hoek-Brown criteria fail to capture the complete extent of brittle behavior according to their analysis. The selection of "s" value becomes essential according to Suorineni et al. (2009) because it requires assessing the characteristics of rock under consideration. Different rock formations exhibit specific intrinsic variations in their strength and fracture behaviors, which cannot be adequately represented by single generic numbers. The usage of generic "s" value restrictions leads to underestimated rock mass strength, which might result in tunnel stability problems, particularly in geologically poor rock masses. Recorded tunnel constructions demonstrate the weaknesses of applying a generic "s" value in the H-B criteria. The 1997 Nantou Second Tunnel excavation encountered compact ground conditions while traversing its total 2.7 km length. The H-B criteria served as the initial stability assessment method with general "s" value set to 1 during this assessment. The use of this underestimated phyllite rock mass's squeezing capability led to an excessive ground deformation, which destroyed the support system. The project experienced budget overruns together with schedule delays because it required extensive rework and additional support installations.

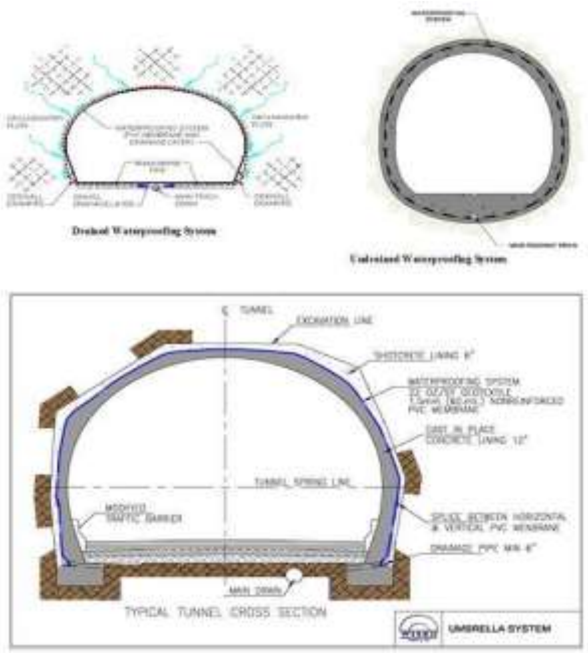

Figure 2. 1 There are two basic types of waterproofing systems: drained (open) and undrained (closed). (Mohammed, 2015)

Jinping II Hydropower Station, China (2010): In this project, a 16.4km tunnel was constructed out of metamorphic rock heavily faulted and fractured. The original concept is based on the foundation of the H-B criteria with a generic "s" value. But during excavation, the rock mass showed more severe fractures and localized stress bursts than the stability limitations that were anticipated. Due to this, the ground support design had to be significantly altered, requiring stronger shotcrete linings and longer rock bolts (Cai et al., 2014).

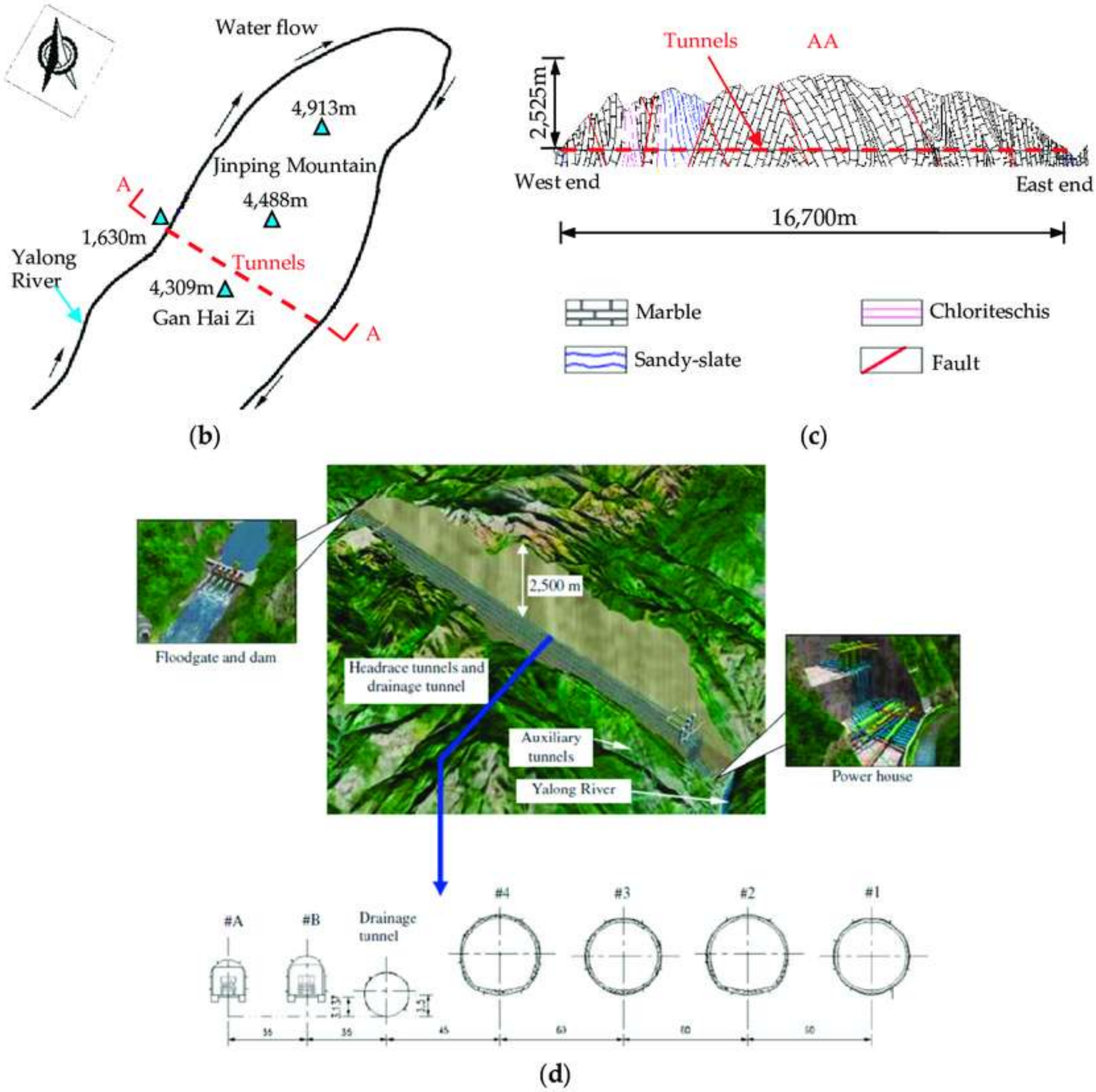

Figure 2. 2 Deep tunnels of Jinping II hydropower station, China. (b) plan of the station, (c) geological cross-section along the tunnels, and (d) layout of the tunnels. (Feng et al., 2019)

These case studies show how an approach to the "s" parameter that is too generalized may result in an underestimate of the strength of the rock mass and possible instability problems.

Using a generic "s" number in the H-B criteria might lead to an underestimation of rock mass strength, which can have dire repercussions. Complete tunnel collapse may occur in severe circumstances if the strength of the rock mass is significantly underestimated. In addition to posing a serious risk to worker safety, this may result in large financial losses from project delays and rebuilding expenses. Existing support mechanisms may fail if the estimated ground support needs are not met because the rock mass strength is underestimated. This may result in squeezing, distortion of the tunnel wall, and perhaps uncontrollable inflows of water or loose rock. Underestimating the strength of the rock mass may lead to tunnel instability episodes that cause worker injuries or deaths. In subterranean construction projects, worker safety depends on precise stability evaluations. Project costs are raised by the need for extra ground support installation, rework because of tunnel instability, and possible delays brought on by safety accidents.

2.3 Methods for characterizing rock mass properties influencing "s"

Creating methods to find "s" values that are particular to a certain rock type requires a better understanding of the characteristics of the rock mass that affect this parameter. The relationship between geological measurements of rock masses and the Hoek-Brown parameters is acknowledged by Hoek et al. (2002). This implies that techniques for geological classification such as rock quality designation (RQD) and discontinuity spacing may be useful in calculating "s". Palmstrom (2005), however, highlights the shortcomings of RQD, especially concerning obtaining precise block size data. A more complete picture of rock mass fracturing and maybe a more precise estimate of "s" might be obtained using other techniques for determining block size, such as volumetric joint count. Determining the Hoek-Brown (H-B) parameter "s" accurately requires a thorough grasp of the characteristics of the rock mass that affect its value. This section examines and contrasts several approaches, both well-established and more recent, for characterizing these traits.

Utilizing the recovery of core samples during drilling, the popular Rock Quality Designation (RQD) technique assigns a grade to the bulk quality of the rock. RQD has drawbacks while being fast and easy. It may not record information regarding larger-scale jointing patterns that might substantially impact the behavior of rock masses since it mainly concentrates on core diameter-sized discontinuities (Palmstrom, 2005). RQD's shortcomings are addressed by the Volumetric Joint Count (J_v) approach, which statistically quantifies the frequency of joints inside a unit volume of rock mass. While J_v may provide a more complete picture of jointing than RQD, it can be time-consuming and needs precise field measurements (Mathews et al., 1990). Rock mass characteristics such as weathering, surface roughness, and joint spacing are included into a single numerical index via the Geological Strength Index (GSI) approach. GSI is often used in combination with the H-B criteria and provides a nice balance between simplicity and detail. But since it depends on subjective field observations, GSI could miss minute differences in the characteristics of the rock mass (Hoek et al., 2002).

Table 2. 1 Comparison of Traditional Rock Mass Characterization Techniques

Method	Strengths	Weaknesses
RQD	Simple, quick	Limited to core diameter-sized discontinuities
Jv	More comprehensive picture of jointing	Time-consuming, requires detailed field measurements
GSI	Balances simplicity and detail, widely used	Relies on subjective field observations

Digital technological developments provide new possibilities for characterizing rock masses: Rock exposures may be converted into high-resolution digital models using methods like photogrammetry and laser scanning. Compared to conventional techniques, these models provide a more objective and thorough characterization of discontinuities by enabling automated joint set detection and analysis (Feng et al., 2013). Numerous factors related to rock mass, such as joint spacing, orientation, and persistence, may be computed using point cloud data obtained by laser scanning. To get a more thorough knowledge of the rock mass fabric, this data may be used with other characterization techniques such as GSI (Wang and Hudson, 2008). Regarding rock mass characterization efficiency, impartiality, and accuracy, these new methods provide a host of benefits. However, the specialized tools and knowledge needed for data collection and analysis may prevent them from being widely used.

The Jinping II Hydropower Station project (discussed above) is a well-researched illustration of how thorough characterization may result in an accurate "s" determination. Here, early tunnel building made the shortcomings of a general "s" value apparent (Cai et al., 2014). A multidisciplinary method was then used by the project team to characterize the rock mass using geological mapping, which included a comprehensive mapping of discontinuity features such as spacing, orientation, and surface roughness. To detect and quantify joint sets, high-resolution digital image processing photos of rock faces were examined. Further details on joint orientation and persistence inside the rock mass were obtained from televiewer pictures captured during the process of borehole image recording. Rock-type specific "s" values were assigned for various geological units encountered throughout the tunnel alignment, and a rock mass categorization system was constructed based on the thorough characterization data. This led to a more precise estimation of the behavior of the rock mass and enabled the construction of targeted ground support, which eventually resulted in the successful completion of the tunnel.

2.4 Geological Strength Index (GSI) and Rock Type Classification

The Geological Strength Index (GSI) empirical correlations provide engineers with a standardized method to estimate rock mass properties through field observation data. The Hoek-Brown failure criterion, together with GSI, allows engineers to determine rock mass strength features as well as deformation behavior for stability assessments in tunnels.

The quantification of rock mass quality depends on GSI because it evaluates joint condition and considers weathering together with block interlocking properties. The classification method helps engineers establish a clear relation between rock mass quality and strength characteristics, which leads to exact parameter assignment in Hoek-Brown models. The GSI-based empirical correlations serve as an effective tool for uniaxial compressive strength (UCS) and deformation modulus estimation because large-scale rock mass laboratory tests are not practical.

GSI demonstrates flexibility when used with various rock types, which strengthens its major significance. The system accepts geological formations spanning from strong igneous rocks through weak sedimentary rocks, thereby achieving more intuitive tunnel stability analysis results.

Through the Geological Strength Index (GSI), petrologists can efficiently determine the "s" value in the Hoek-Brown failure criterion that defines the non-linear strength attribute of fractured rock masses. The GSI assessment method incorporates human evaluations of rock structural elements together with the condition of discontinuity surfaces to quantify rock mass quality attributes. The "s" parameter can be determined through an exponential empirical relationship when they incorporate the disturbance factor (D) to measure the mechanical damage effect from blasting or stress relief events, as it was shown in Equation 1.3. The method facilitates engineers to evaluate complex rock mass reactions through calculations without depending on comprehensive laboratory tests, especially for early design phases and field conditions. GSI-based correlations have the main advantage of being relatively straightforward to apply during fieldwork processes. The GSI assessment method provides an engineer with a fast, practical, and simple way to assess the stability of rock masses at tunnel construction sites without the need for expensive equipment to achieve this.

2.5 Importance of rock mass characterization for accurate "s" determination

A thorough description of the rock mass is needed to determine the Hoek-Brown parameter "s" accurately. Specifically, Senent et al. (2013) highlight the role of the characteristics of the rock mass represented by the parameters of the Hoek-Brown in the stability assessment of the tunnel face, particularly in the case of highly fragmented rock. They mention the need to take these features into account when excavating tunnels to maintain stability. Suorineni et al. (2009) provide a method of calculating rock type-specific "s" values based upon rock attributes that can be quantified. This method highlights the need for thorough rock mass characterization before the determination of suitable 's' values that accurately represent different rock types. Hoek et al. (2002) studied that the Hoek-Brown (H-B) failure criteria is important in the behavior of rock masses by estimating the scope of possible failure zones around a tunnel. This criterion contains many characteristics, but this "s" parameter signifies the necessary conditions for the strength of rock mass and the outcome of the brittle behavior (Martin et al., 1999). Invariably, “s” has been given a generic value of “1” (Hoek et al., 2002), regardless of the type of rock. However, in geologically complex situations, this method can lead to wrong evaluations of stability (Suorineni et al., 2009). This literature review emphasizes the significance of proper rock mass characterization for the selection of 's', and also considers the influence of geological variables and rock mass fabric.

As stated by Hoek et al. (2013) the rock mass fabric refers to the twenty how big or determined spatial organization of all structuring constituents in a rock mass: blank is included (faults, joints), intact rock physical properties (strength, grain, mineralogy), respective extent of weathering and modifies. Interaction of this nature has a large influence on the mechanical behavior of the rock mass (Mathews et al., 1990). An example is closely spaced, persistent discontinuities, which may dramatically affect overall strength and stiffness (Palmstrom, 2005). However, rock masses with fewer fractures and stronger intact rock features will show more ductile behavior. To choose the right "s" value, one must know about the rock mass fabric. Rock types with more dominating fabric of discontinuities, as opposed to rock types with minor fractures, tend to have more brittle behavior and need a larger (Martin et al., 1999). (Renani & Cai, 2021) emphasize the significance of this idea for the Jinping II Hydropower Station project. The latter became highly unstable for the project, which was initially based on a generic 's' value but was found to have an unanticipated fracture. Characterization of the rock mass from discontinuity mapping and digital image processing allowed the determining of the "s" values specific to each type of rock and completing the tunnel.

The characteristics of weathering, alteration, and the presence of faults and fractures of rock mass need to be considered to accurately determine the "s" value of a rock mass. Weathering processes can break the rock mass by decreasing the strength and integrity of discontinuities and intact rock, as described by Hoek et al. (2002). Suorineni et al. (2009) state that the value of "s" increases with the weathering of highly weathered formations and decreases with the weathering of fresh, unweathered rocks. An example of alteration that may change the original mineralogy of the rock or give rise to additional secondary minerals that might affect the mechanical behavior is hydrothermal activity (Hoek et al., 2002). This requires changing the value of the s, which depends on the specific kind of alteration that occurred and its impact on the strength of the rock. Faults and fractures are areas of weakness in the rock mass and have a significant impact on the overall stability of the rock mass (Brady and Brown, 2006). When deciding upon the 's' value for grouting after excavation, attention must be paid to their (i.e., the grouted objects) existence, features (size, orientation, infilling characteristics), and any interactions with the tunnel's planned alignment. However, engineers can carefully account for these elements throughout the rock mass characterization process and choose an 's' value that accurately represents the particular geological circumstances that have been found and have a more nuanced knowledge of the behavior of the rock mass.

2.6 Validation of methods for rock-type specific "s" values

The implementation of rock-type specific "s" value calculation methodologies needs complete testing before they can be used practically. The study performed by Suorineni et al. (2009) uses quantifiable characteristics of rocks, while additional testing needs to confirm its effectiveness across multiple rock compositions and site locations. The validation process, together with "s" value assessment and in situ rock mass monitoring, should be assessed through laboratory testing of complete rock core material. Rock mass characterization data presents crucial value when forecasting rock material behavior under stress, according to Brady and Brown (2006). Current knowledge about rock properties and fracture properties of different rock types results from performing rock core analysis in laboratory conditions that maintain strict control. Laboratory tests of rock samples combined with appropriate correlation to identification methods will enhance "s" selection models for specific rock types. Engineering professionals use the H-B failure criteria as part of their standard practice to predict tunnel failure zones (Hoek in al., 2002). The "s" parameter functions as the critical factor in the criteria that enables both rock mass behavior analysis and brittle failure pattern prediction (Martin et al., 1999). Modern practice includes assigning the "s" value as "1" without considering rock type classification by Hoek et al. (2002). According to Suorineni et al. (2009) improper selection of this method produces inaccurate stability predictions, particularly when complex geological conditions are present. The precision of H-B estimations improves when researchers establish specific "s" values through the complete characterization of different rock types according to previous research (Renani & Cai, 2021). This literature review examines how rock-type specific "s" values become difficult to validate through verification techniques along with discussing potential uses of back analysis in verification methods. The research paper proposes specific requirements related to future study in its field.

Multiple substantial challenges emerge during the process of validating techniques for estimating rock-type specific "s" values, which stem from limited case studies and diverse rock types, and collecting in-situ data. Surface measurements of rock mass behavior represent the main obstacle in research efforts. Traditional core sample laboratory tests fail to properly identify the complete relationship between underground stress conditions and discontinuities (Brady and Brown, 2006). The implementation scale-up of borehole shear in-situ testing techniques proves time-consuming and costly, according to Mathews et al. (1990). The same rock type shows significant variations between its weathering properties and strength levels and patterns of fracturing (Hoek et al., 2013). Efforts to develop universal "s" calculation methods for multiple expressions of a single rock type are prevented by each rock example's unique characteristics. The validity of modern "s" measurement approaches gets established by observing tunnel activity in different geological formations against calculated model results. According to Read and Richards (2015), there is a shortage of detailed case research that tracks the actual tunnel construction period and provides detailed rock mass characterization records. A strong validation plan should accompany the development of rock-specific methods used to determine "s" value due to these difficulties.

Back analysis serves as a verification tool for testing procedures that determine "s" value in rock-based materials. The assessment of suggested procedures requires observers to compare existing tunnels' behavior in different rock environments. The analysis consists of three main parts that include data collection followed by application, then analysis of observed versus expected outcomes. Research and document the current tunnel observation data regarding support requirements and stability challenges while recording rock mass attributes, including discontinuity intervals and rock quality features (Renani & Cai, 2021). Use the chosen method to obtain rock-type dedicated values of "s" that correspond to each investigation tunnel by consolidating its rock mass characterization data. An evaluation should be conducted to compare predicted "s" values with the real ground support requirements and construction-related stability issues that developed during the tunnel building stage (Suorineni et al., 2009). Scientists can enhance the calculation methods for "s" values through research study that identifies discrepancies between estimated and observed actions. The research cycle has the potential to produce improved methods for selecting "s" values for specific rock formations.

Some areas that need further investigation to further verify methodologies for obtaining rock type particular 's' values include standardized in-situ testing, sophisticated characterization techniques, and case study databases. Standardized in situ testing techniques are needed to be able to depict precisely the behavior of rock masses influenced by discontinuities and stress conditions. These should be reasonable and useful techniques with which to proceed in actual use in tunnel construction (Mathews et al., 1990). For a given rock mass classification such as HH damage (GSI), the use of the cutting-edge technology for precise rock mass characterization (such as digital image processing and point cloud analysis) can bring more thorough data for 's' determination (Feng et al., 2013). There are many correlations to be made between these characterization methods and the mechanical properties of different types of rock that will require further investigation. The establishment of a centralized database of well-documented tunnel projects that includes observations of behavior and precise data on rock mass characterization would, back examination and validation of "s" determination techniques, go some way to improving (Read and Richards, 2015). Therefore, researchers would be able to examine more case studies and be able to generalize their findings more widely. Furthermore, the H-B is used to meet those research objectives and continually improve techniques, which tend to yield different groups of "s" values for various rock types.

2.7 Potential Benefits of Rock-Type Specific "s" Values for Tunnel Stability Assessment

Particularly defined "s" values for each type of rock would aid in making tunnel stability evaluations much more accurate and reliable. Therefore, engineers may get more precise estimates of the failure zones possible around tunnels when rock strength and fracture behavior differ within different rock formations. This allows the planning of ground support that is more focused and successful. The importance of including the characteristics of rock mass in the excavation of tunnels as a measure of maintaining stability is emphasized by Senent et al., (2013). 'Engineering may use 's' values unique to a particular kind of rock to tailor the ground support measure to the behavior of a rock mass that they know or expect to meet. It indicates the sound support design and potentially reduces costs for the entire project. In addition, accurate stability evaluations may also decrease the possibility of tunnel collapse and attendant risk to the safety of construction workers.

Hoek et al., (2002) state that the Hoek-Brown (H-B) failure criteria is necessary for assessing the behavior of rock masses and predicting potential sites of failure around tunnels. Martin et al., (1999) insist that the 's' component of such criteria is essential in the strength of the rock mass and forecasts brittle behavior. For instance, just in the case of the type of rock, the generic value of "s" is historically "1" (Hoek et al., 2002). However, this method results in erroneous stability estimates and thus expensive project delays, safety risks (Suorineni et al., 2009). In recent studies, such increased accuracy of H-B forecasts for tunnel building projects has been found to greatly increase with the use of rock-type specific "s" values ascertained by thorough characterization.

Rock-type specific “s” values have financial benefits such as lower ground support costs, fewer construction delays, and fewer worker accidents. Engineers can design ground support plans that are optimal by creating ground support plans with suitable stability evaluations from "s" values that are characteristic to each kind of rock. It is thus that a decrease of shotcrete, rock bolts, and other support measures may be needed, thereby resulting in a significant amount of money saved (Renani & Cai, 2021). Unanticipated tunnel instability occurrences may be brought on by an underestimate of rock mass strength, leading to project delays and rework. The use of rock type-specific 's' values allows engineers to anticipate potential stability problems more precisely for preventative steps and spending that which is expensive in terms of delays (Feng et al., 2013). Worker safety from tunnel collapses and ground support failures is a danger. Reduction of these types of occurrences may help to make the workplace safer and perhaps decrease the number of worker compensation claims. This can be done with accurate stability evaluations based on rock type-specific 's' value.

The impact on the environment is considerable in the building sector. Optimization of ground support systems based on ground support stability assessments with rock type-specific 's' values can provide a reduction in material consumption, minimization of energy consumption, and generation of less waste. Optimized design offers reduced environmental effects from material extraction, processing, and transportation, as less material is used for ground support (Read and Richards, 2015). Ground support materials must be used for the manufacture and delivery of energy. Using less material (Mohammed et al., 2020) will reduce the total energy footprint of the project. During the tunnel construction or after its completion, trash might be generated from unsuitable or excessive ground support. The use of rock type-specific “s” values for tunnel stability evaluations provides economic and environmental benefits that support its use.

It shows several case studies of how rock type-specific “s” values work in actual tunnel building projects. (2010) Jinping II Hydropower Station, China – using a generic “s” value, this project had serious instability problems. Upon the detailed characterization of the rock mass, the project team could effectively finish the tunnel by changing ground support tactics after the 's' values for each kind of rock were determined (Cai et al., 2014). Compressing ground conditions were unanticipated in another project, Taiwan's Nantou Second Tunnel (1997), as the 's' number was used to underestimate rock mass strength. These problems may have been averted, and project delays and costs could have been minimized by appropriate implementation of rock type-specific "s" values derived from good characterization. The results from these case studies illustrate that 's' values based on rock type are useful in the civil construction business to achieve the desired results at minimal cost. This literature study systematically studies the significance of rock type-specific “s” value for more precise tunnel stability evaluation through the cost and benefit analysis, reviewing the environmental impacts, and provides the practical case studies. Research on standardized in situ testing methodologies, enhanced rock mass characterization techniques, and the development of case study databases would further strengthen this approach in the area of rock engineering.

The overall conclusion is that rock type-specific "s" values have a great potential in the science of tunnel stability evaluation. Improving methods for identifying 's' and for verifying them during extensive testing may facilitate a broader practical implementation of this technique by researchers. The possible advantages include improved ground support design, more secure stability forecasts, and eventually, safer and more affordable tunnel building projects.

3 RISK MANAGEMENT

3.1 Overview of Risk Management

Projects that utilize the Hoek-Brown failure criterion encounter physical and operational hazards throughout the processes of “s” parameter estimation and Geological Strength Index evaluation and Acoustic Emission testing and thin section preparation and Uniaxial Compressive Strength analysis. High-pressure equipment use together with field sampling in unstable terrains and exposure to chemicals and the use of machinery and instrumentation produce these hazards. Users of risk management systems achieve safety and data quality and project timeliness through effective identification and evaluation and hazard mitigation procedures. The main physical risks for different project stages are described in detail in this section, where the hazard ratings and probabilities from Table 3. 1 and Table 3. 2, along with a condensed Hazard Identification and Risk Assessment Table, are presented.

Table 3. 1 Hazard Impact Rating

Consequence	Explanation
Catastrophic	The project could not be completed due to serious issues
Major	Significant delay in project delivery due to data loss
Moderate	Probable delay in project delivery due to solving the issue
Minor	Little issues on project delivery; work is continued without delay
Negligible	The project is impacted insignificantly, work is continued

Table 3. 2 Probability Scale

Probability	Explanation
Almost Certain	Expected to occur in most circumstances
Likely	Will probably occur in most circumstances
Possible	It might occur at some time
Unlikely	Could occur at some time
Rare	May occur only in exceptional circumstances

3.2 Physical Hazards

This work contains physical elements that comprise rock mass sampling and laboratory testing alongside analytical instrumentation, and these features produce different dangers that affect safety alongside equipment durability and ongoing project operations. The activities need individual protective procedures to control risks effectively. Table 3. 3 contains the complete listing of hazard consequences along with their associated probabilities as well as complete lists of applicable control methods.

Table 3. 3 Hazard Identification and Risk Assessment

Activity	Hazard	Potential Consequence	Impact Rating	Mitigation Measures
Field Sampling and GSI Assessment	Falling rocks, slips/trips, musculoskeletal injuries from lifting, tool-related injuries.	Project delay, injury, or data quality issues	Moderate	Use of helmets, boots, gloves, field training, weather monitoring, buddy system.
Thin Section Preparation	Exposure to silica dust, sharp blades, chemical inhalation (epoxy, acetone), machine entanglement.	Project delay, injury, or data quality issues	Minor	Fume hoods, PPE (masks, goggles, gloves), proper ventilation, machinery guards.
UCS Testing	Rock fragment ejection, high axial stress equipment failure, pinch injuries.	Project delay, injury, or data quality issues	Major	Use of shielding cages, distance protocols, emergency stop systems, trained operators.
AE Monitoring	Electrical hazards, cable entanglement, sensor damage, equipment sensitivity.	Project delay, injury, or data quality issues	Minor to Moderate	Cable management, proper grounding, clean workstations, training on AE setup.
Chemical Handling	Skin/eye irritation, chemical burns, VOC inhalation, fire hazard.	Project delay, injury, or data quality issues	Minor	Chemical storage compliance, PPE, fume hoods, MSDS availability, spill response.

3.3 Contingency Plans

Any research project in geotechnical or rock mechanics faces unexpected challenges that exist despite well-developed planning and risk control methods. This work continuity with high-quality data, along with personnel safety, depends heavily on the development of strong contingency plans. This part specifies crisis management protocols that address field sample collection and laboratory assessment of uniaxial compressive strength and thin section processing as well as instrument operation for Acoustic Emission testing since these activities provide crucial data for determining Hoek-Brown “s” parameter and GSI.

If fieldwork is delayed owing to challenging weather, access limits, or safety threats (e.g., unstable slopes), alternate locations with equivalent lithological and structural characteristics will be identified ahead of time using geological maps and remote sensing data. Sample duplication and detailed field images, along with geologic notes, will back up missing data when a portion of rock samples becomes unusable. GSI estimation can continue temporarily through core-based assessments or photogrammetric analysis when entire field access is denied.

Analysis failure through petrography can result from sample breakage during cutting or polishing or epoxy curing failures, or equipment delay incidents. A strategy includes the preparation of multiple rock billets at once to serve as backup items. A dedicated stockpile of embedding materials together with resins will stay as backups against material scarcity. The company has established in advance arrangements to contact outside labs for thin-section preparation work when equipment needs maintenance or breaks down. Any malfunction in testing equipment or geometrical defects in the samples can lead to UCS testing failure. The ASTM or ISRM standards will be used to check test specimens before the loading process to prevent data loss. The scheduled scheduling of UCS tests with an affiliated laboratory will start when UCS equipment becomes temporarily unavailable. Furthermore, indirect strength parameters (e.g., Schmidt hammer rebound, Brazilian tensile strength) may be used for correlation-based estimation as a supplementary method.

The proper handling of chemicals and safety measures receive continuous reinforcement because all areas contain spill response kits together with first aid equipment and contact information. The laboratory operations will stop during incidents before they can restart based on incident report evaluations and safety assessment completions. The plans guarantee data acquisition and analysis integrity for rock mass characteristics and mechanical modeling which supports the successful obtaining of Hoek-Brown parameters.

4 METHODOLOGY

A systematic evaluation of rock-type-specific Hoek-Brown parameter “s” through this investigation leads to enhanced tunnel stability. A three-step protocol starts with gathering data and then preparing samples before subjecting them to laboratory tests that measure rock mass geomechanical characteristics. Mapping rocks and core examination work carried out in detail should be for document rock formations along with joint system features that affect the rock deformation behavior. The core logging supplies vital information regarding rock classification, weathering state and discontinuity, which is useful in selection of right sample assaying types. The data preparation segment is sample core preparation using thin section analysis. To achieve reliability of testing through flat and parallel ends, the core samples are sliced into cylindrical shapes according to ISRM standards with the ratio of diameter to length of 1:2. Stress strain analysis on continuous stress and deformation data acquired during testing of prepared specimens, are used in UCS, to measure σc and σci. Thin sections prepared from normal rock specimens are used for mineralogical composition and microstructural characteristics examination. However, through three steps of processing, petrographic microscope examination is now available on new technological handling, which results in prepared rock specimens of uniform thickness of 0.03mm. Microscopic examination of the rock allows to see the rock's internal structure and to determine the bonding and fail pattern of mineral that affect the rock's strength properties.

4.1 Materials and Methods

This approach integrates field geological data collection with laboratory analysis to conduct a comprehensive evaluation of the Hoek-Brown parameter "s" resulting in enhanced estimates of tunnel stability specific to rock types. The examination of rock behavior and predictive modelling is enhanced by the integration of macroscopic field studies and microscopic petrographic research methodologies.

4.1.1 Rock preparation

Preparation standards used for this study for uniaxial compressive strength measurements have been met with rock samples of fine-grain sandstone and coarse-grain sandstone. Cylindrical core samples were extracted from bulk sandstone blocks using a diamond core drill to have the geometry more consistent and reduce sample variability. The initial diameter of each core was 63 mm.

The yield strength values from the UCS measurements became more reliable after using standard ISRM-recommended core specimen cuts with a length to diameter 2:1. Grinding and polishing specimen ends were performed precisely to limit stress concentrations during loading until both ends were within specifications to plus and ±0.02 millimeters parallelism and ±0.05 millimeters flatness.

The mechanical behavior testing of sandstone samples required specimens to undergo oven drying at 105°C for a minimum period of 24 hours until all moisture content reached zero levels. A controlled environment was used for storing specimens after drying to maintain stable temperature and humidity conditions that stopped the alteration of material properties before testing. During UCS testing, accurate stress straining data were taken with a servo-controlled loading frame having strain gauge equipment. It used strain gauges attached to specimen surfaces to measure both axial and lateral movement under load for calculating limits of failure onset and mechanical behavior. The established methodology produces reliable results that enhance the predictability of Hoek-Brown's "s" parameters in performing underground construction stability assessments. The uniaxial compression testing needed both ends of each core specimen to be properly polished until they became flat symmetrical, parallel surfaces to create uniform stress distribution. Both ends required surface preparation with different sandpaper grades until they reached a smooth finish. The proper surface preparation represents a crucial requirement because it reduces stress concentrations, which results in precise strain readings.

After surface polishing of end surfaces reached adequate standards the attachment region received additional treatment for better adhesive bind. The surface received chemical solutions that function to promote core-adhesive bonding despite the study not revealing the specific solution composition.

The core specimens received surface treatment before strain gauges got applied through high-strength adhesive. An extra step was included to guarantee correct axial alignment of all gauges. Each strain gauge received electrical connection to a preconfigured circuit with signal wires that ended at a Digital Strain Display (SM1010). The experimental setup utilizes the wiring diagram along with circuit diagram which is shown in Appendix A.

The system testing concluded with electrical connection integrity checks followed by equipment operational readiness confirmation before specimen UCS testing commenced. The device measured strain values in real time during the test period to monitor the stress-strain relationships and axial load data synchronized together.

Figure 4.1 Example of rock sample preparation for the test: a) example of delivered cores, b) prepared rock samples for UCS test

4.2 Acoustic Emission

4.2.1 Method justification

The use of acoustic emission (AE) technology has proven to be a powerful means of determining critical stress threshold value of rocks. Monitoring the acoustic emissions produced with rock deformation and fracture processes allows researchers to gain information regarding the changes in the internal structure and impending rock mass failure. AE has gained much attention in the field of rock mechanics and engineering through several studies. Identifying stress thresholds in rocks is one of the more common places that AE is heavily used. Zhao et al. (2020) have used AE technology to identify stress thresholds for the rock loading process in the uniaxial compression tests performed on granite samples. However, research showed that by analyzing the characteristic parameters of AE activity, the threshold values can be determined at different stages of rock deformation prior to the peak pressure. It offers a practical way for understanding the stress levels which must be exceeded to cause a significant change in what would otherwise be considered rock failure. Cai et al. Zhang et al. (2023) further developed a method to calculate rock mass strength parameters using generalized AE thresholds and finite element stress analysis. Due to the ability to use AE monitoring data to learn the important strength parameters in this method, this method is proposed as a comprehensive way to evaluate rock stability as well as rock potential for failure. On top of that, Zhang (2018) focused on the AE technology's real time monitoring ability on recording rock fracture processes. Researcher can effectively monitor the rock instability and failure progression by analyzing AE time frequency parameters to understand the rocks under stress. Finally, the application of AE technology in rock mechanics has greatly changed the approach to the determination of critical stress thresholds of rocks. Researchers can use these acoustic emissions produced during rock deformation and fracture to determine stress levels, anticipate failure or predict behavior of rock under different stress conditions. The AE data is interpreted based on the application of AE test. Three methods to solve the problem of where the crack start in rock are formed. The next techniques are determining the stress whereby cracks are formed.

- The point of inflection of the lateral strain-axial stress curve (Bieniawski,1979)
- At the point where the fracture volumetric strain starts to rise (Martin, 1993)
- Second inflection point on linear section of volumetric stiffness - axial stress curve, where second change of slope (Eberhardt 1998).

These approaches are used to obtain crack initiation stresses which are verified by plotting the axial stress versus the acoustic emission (AE) events. The Martin's method for determination the stress at which cracks start to form was chosen in this work.

4.2.2 Equipment

In this study, the acoustic emission approach was implemented based on the SAEU3H AE system developed by QingCheng AE Institute (Guangzhou) Co., Ltd. The picture below is the arrangement of the equipment. It consists of AE data collection modules, an optional network connection module, a computer, sensors/preamplifiers/cables (AE Institute Co., Ltd., 2017). For instance, out of the sensors available during the test, only sensors 1 through 4 are used. The reason is that the remaining sensors cannot be used as the height of the rock samples limits their application. Additionally, the acquisition of data from acoustic emission sensors is enabled by the use of SWAE, software used to collect data.

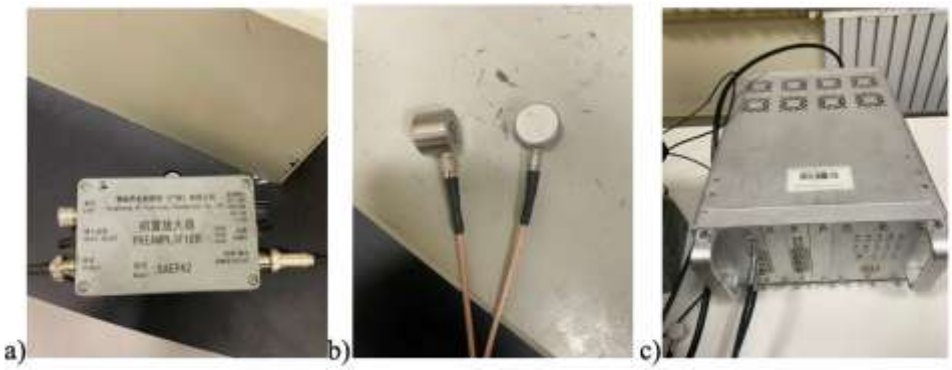

Figure 4.2. Acoustic emission equipment; a) preamplifier, b) sensors, c) power unit

4.2.3 Testing procedure

Sensors were attached to the surfaces of specimens with hot glue in order to maximally acoustic couple. The use of hot glue facilitates the secure attachment of sensors, so ensuring their continuous contact with the rocks. In the process of taking data the sampling rate should be set to 1 MHz, the trigger threshold and pre-amplified gain should be set to 40 dB. However, while this saw the acquisition of background noise, and more than 500,000 data points, this was only to a threshold value of 40 dB, as this is the point at which listening would become unmusical. Therefore, the threshold of the test has been set at 55 dB and up to 60 dB in some instances.

The unprocessed data that came from the trial is stored in a form of Microsoft Excel file. The generated output file has a column structure of arrival time, AE channel, amplitude (dB) counts, duration, energy, rise counts, rise time.

4.3 Thin section preparation

The two representative sandstone rock samples which were obtained in the field for petrographic analysis, were used to prepare their thin sections. Diagenetic features were examined in fine-grained and coarse grained sandstone core specimens by thin sections. During sample preparation, first, rectangular rock pieces are made by a precision saw, which is smooth in parallel surfaces and flat surface. With a hammer and chisel, further rock sections were removed to avoid thin sections from damaging the main sample and to prevent the main sample from being damaged mechanically. Then, the water was applied with a soft bristled brush for removal of all debris and dust that might remain after the cutting, after which all samples were sliced through the cutting process. Full airflow drying was performed on the produced samples to protect them from contaminants to the following mounting processes.

The prepared samples were lightly covered with epoxy resin, spread on the glass slides and the samples were placed therein. Sandstone chips were affected mainly by their brittle nature and weak texture of coarse grained materials and a process of epoxy resin impregnation was required. As an additive, epoxy was chosen since it allowed the refractive index of 1.54 to maintain the pore structure while preventing the development of cracks in processing. In infiltration carried out using the vacuum embedding unit, ten samples were simultaneously embedded under isothermal conditions up to 80°C, maintained with the unit. Vacuuming with procedures that reduced the viscosity of epoxy stemmed from air bubbles with the focus on filling pores to improve sample quality and optical transparency. The adhesive helped immobilize specimens on glass slides by being attached to this surface on the bottom of a specimen. This was done by treating the surface of the specimens for superior stability.

Figure 4.2 shows the procedure of rock sample being attached to glass slides for petrologic examination through thin section preparation. Since sandstone cannot be embedded in epoxy, the Montaging procedure for glass slide attachment is necessary to maintain sample connectedness and structural soundness and, at the same time, necessary optical clarity for accurate imaging.

To know what you're cutting and be able not only to adjust the cutting precisely, but also to cut with precisely 200 µm (but less than 200 µm) thin sections, the slicing machine was used with a precision saw that cuts the specimens with a digital micrometer with a resolution of 5 µm. The vibration free base system in conjunction with the vacuum chuck, was able to accomplish damage free cutting of fine grained sandstone pieces.

When the adhesive hardened, thin samples (30 micrometers) of mounted samples were generated by precision rock saw and these thin sections were imaged. The sample was left intact by allowing the sections to be cut perpendicular to the glued surface. The thin sections were received on glass slides which were subjected to several consecutive steps of polishing with application of Canada balsam as the clear adhesive. Since the cross-sectional thicknesses of the sections were to be within the range of 0.15 – 0.03 mm finite thickness, the problems of sandpaper and polishing wheels to achieve gradually reduced sample thicknesses were addressed. A thin section lapping jig enabled precise orientation and control of samples as well as a utility of an unevenness correction rim that was flattened and aligned across all samples.

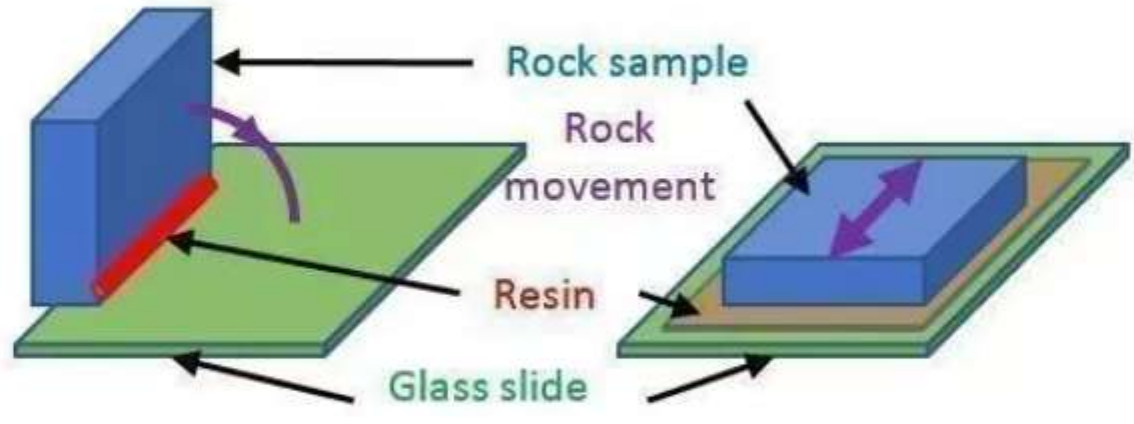

Figure 4.3 The process of mounting a rock sample onto a glass slide for thin section preparation

A schematic representation of the thin section preparation process is provided in Table 4.1 The methodical section preparation produced top-quality sections that helped researchers investigate essential characteristics of pore structure and diagenetic features and mineralogical content of fine-grained and coarse-grained sandstone compositions for behavioral studies.

Table 4.1 Thin Section Preparation Workflow

Step	Procedure	Equipment Used
1	Cutting of sample	Cutting saw
2	Resin impregnation of sample, if necessary	Embedding machine
3	Trimming of sample	Polishing machine
4	Lapping of sample	Lapping machine
5	Flat thinning and lapping of glass sample holder	Lapping machine
6	Bonding of sample on glass sample-holder	Bonding set
7	Slicing at 100–500 μm	Slicing machine
8	Grinding at 30–35 μm	Grinding machine
9	Final polishing	Polishing machine

4.4. Uniaxial compressive strength

It is hard to predict or measure rock properly, and it is a tough job to understand the failure mode of rock. Therefore, it is important to examine the failure mechanism of rock by conducting UCS testing on several rock types in this study. This portion of the research provides an explanation for the selection of laboratory equipment and details the experimental setups and test processes.

The researchers successfully determined the stress thresholds for crack initiation (σci) and crack damage (σcd), which are essential factors in the brittle fracture process. Furthermore, the testing findings demonstrated substantial differences in the characteristics of the acoustic events throughout the loading process, namely before to and after the onset of cracks. Eberhardt et al. (1997) state that researching the fracture processes in laboratory tested rock may improve our comprehension of how generated stresses in the rock around an excavation lead to the decreasing of strength and failure of the surrounding rock.

The uniaxial compressive strength (UCS) tests were conducted following ISRM-recommended procedures to determine the strength and deformation characteristics of sandstone. Each prepared core specimen was placed in the axial alignment within the platens of a servocontrolled compression testing machine, and there was careful eccentric loading was avoided. The load was applied at a constant displacement rate between 0.5 and 1 mm/min until the specimen failed. Then, from the peak load at failure, UCS was calculated using the formula:

$$\sigma_c = \frac{P_{max}}{A} \quad (3.1)$$

The UCS is given by σ_c (MPa), P_{max} (N), and A (mm2) is the cross-section area of the specimen.

High-precision strain gauges (Digital Strain Display SM1010) were attached to the specimens on the axial and lateral directions to do strain responses during loading. These gauges measured real-time deformations, allowing for the calculation of key mechanical parameters such as Young's modulus and Poisson's ratio. Young's modulus was determined using the stress-strain relationship in the linear elastic region of the stress-strain curve:

$$E = \frac{\Delta\sigma}{\Delta\varepsilon} \quad (3.2)$$

where $\Delta\sigma$ is the change in axial stress and $\Delta\varepsilon$ is the corresponding change in axial strain.

Then Poisson's ratio (v) was computed as:

$$v = -\frac{\varepsilon_r}{\varepsilon_a} \quad (3.3)$$

where ε_r is the radial strain and ε_a is the axial strain.

The strain gauge data were continuously recorded and analyzed to assess rock deformation behavior, stress-strain relationships, and failure characteristics. This combined approach of UCS testing and strain gauge analysis provided a comprehensive evaluation of the mechanical properties of fine-grained and coarse-grained sandstone, forming the basis for refining the Hoek-Brown *s* parameter in this study.

4.4.1 Equipment

For this research, compressive strength test was performed on cylindrical rock samples by using GCTS Uniaxial Testing System UCT 1000. Maximum axial load capacity of the machine is 4500 kN. It has also ability of moving up to 200mm in axial direction. The load frame is a four column frame with subsequent crosshead adjustments and a frame stiffness up to 5000 kN/mm. Both static and dynamic testing is performed by the machine that uses electrohydraulic, closed loop digital servocontrol applied to axial load or deformation. The on specimen axial and radial strain measurement system was used for this research. For data acquisition (Unconfined Compression - GCTS Testing Systems, 2021), during the testing, the custom built Microsoft based software by GCTS Testing is used.

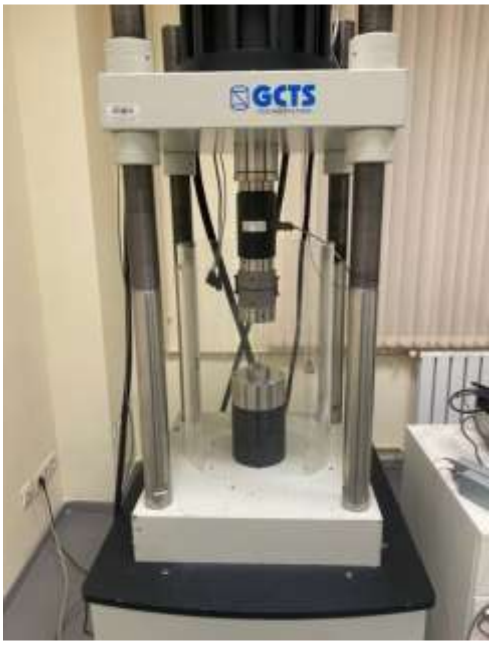

Figure 4. 4 GCTS testing system, UCT-1000

Uniaxial compression tests were carried out on rock samples (having fine or coarse grain size). In these tests, failure of the samples was achieved by loading them until failure while strain gauges measuring when microstrains ($\mu\varepsilon$) were induced in the specimen surfaces recorded deformation. Two key stress parameters for the test were provided.

Uniaxial Compressive Strength (UCS, σ_c): Maximum stress which was obtained at the point when the specimen failed.

Damage Initiation Stress (σ_{ci}): The stress at which damage initiation can be detected (i.e the stress at which the recorded strain curve deviates from linearity).

Under compression, the deformation of a typical rock is characterized by an initial linears elastic deformation. The strain gauge readings tend to behave according to some linear trend (often graphically indicated as "damage initiation") but at some stress level deviate from this trend (often indicated on graphs as damage initiation point). The onset of micro-cracking in the rock is associated with this deviation, of which the axial strain versus stress or the lateral strain response method (LSRM) may be used.

The lateral strain response method (LSRM) is employed to determine the damage initiation stress (σci) and the location on the stress–strain curve at which the lateral strain becomes different than the first linear elastic trend initiating microcracking. To compute s from the formula, Hoek–Brown brittle constant s is calculated after knowing σci using LSRM.

$$s = \left(\frac{\sigma_{ci}}{\sigma_c}\right)^2 \tag{4.1}$$

These three are represented byσc: uniaxial compressive strength (UCS), namely, the maximum stress that the rock can withstand. A quantitatively measure of the proximity of the damage initiation point to the UCS, this parameter (s) is used judiciously to determine stability and design of geotechnical structures as heuristically demonstrated by its use in the brittleness of s .

4.5 Data analysis

Data analysis through field observations as well as laboratory test results and petrographic studies enables the refinement of rock-type-specific Hoek-Brown parameter "s" for better tunnel stability outcomes. The analysis system uses a systematic method starting from the interpretation of geological maps and core documentation for rock classification, joint analysis, and rock mass evaluation. Laboratory findings work together with geological information to explain the connection between structural rock features and their strength characteristics.

The UCS test results lead to the calculation of peak stress values and damage initiation stress measurements during mechanical analysis. The evaluation of rock deformation by each rock type relies on stress-strain curves, while acoustic emission data help trace microcracking along with failure progression. The UCS values become fundamental to determining the material constant "s" for rocks through the Hoek-Brown failure criterion, which takes account of structural and grain size effects. The measurements obtained from the "s" calculations undergo verification against established empirical fundamental relations to measure model accuracy.

Petrographic analysis of thin sections provides insights into the mineralogical composition, fabric, and microstructural characteristics affecting rock strength. The degree of mineral interlocking, along with the presence of microfractures and all observed alteration features, is documented and correlated to the UCS test results. The microstructural evaluation assists mechanical test interpretation through the mineralogical and textural identification of rock failure mechanics.

The developed methodology creates specific rock-type assessments of tunnel stability which improves the accuracy of geotechnical predictive models for engineering applications.

4.6 Test arrangements

The section describes how experimental design was implemented to study sandstone samples under uniaxial compressive stress. The work is focused on Acoustic Emission monitoring and strain measurements form the basis of this investigation because they detect damage initiation as well as characterize the 's' values of the brittle Hoek-Brown constant. All tests were conducted following the ISRM criteria for executing UCS tests.

The evaluation measured ten cylindrical samples composed of coarse-grained and fine-grained sandstone. The testing method abided by ISRM recommendations through utilizing samples with 2:1 length-to-diameter dimensions. The grinding process of end faces aimed to produce flat surfaces parallel to each other, which generated uniform loading distribution. The uniaxial compression machine positioned the samples in vertical orientation between its loading platens. The testing machine applied load to each specimen using a steady displacement pace of 0.5 mm/min before it failed. The synchronization between strain and AE data collection allowed researchers to measure UCS, εci, σci, and finally obtain the brittle Hoek-Brown constants.

4.6.1 AE arrangements

Acoustic Emission monitoring serves as a vital non-destructive method that detects microcracks that form while monitoring rock materials under loading conditions. This research involved mounting AE sensors directly on sandstone core surfaces to detect high-frequency elastic wave emissions from evolving and forming microcracks. Electrical signals emerge from elastic waves detected by these sensors to identify the damage initiation point, which scientists also name microcracking onset. The AE system operated with two piezoelectric AE sensors, which had a frequency bandwidth of 100–400 kHz while they were connected across from each other to a cylindrical rock specimen through the application of couplant gel for signal transfer optimization. The testing period required the secure attachment of sensors with combinations of rubber bands and sensor holders to provide stable sensor contact. The pre-amplifier functioned with a gain level set to 40 dB for better signal precision. AE data acquisition systems incorporate dedicated software to view and process real-time signals while having typical capabilities across 4 channels. Avoiding interruptions UCS testing enabled the collection of AE information that included frequent measurements of AE event numbers plus amplitude levels and energy signatures along with signal intensity values. AE activity showed a link to stress levels, which allowed researchers to determine damage initiation stress (σci) as the precise stress for microcrack initiation. The correct determination of the 's' parameter requires this particular stress measurement.

4.6.2 Strain measurement arrangements

The strain gauge data was measured simultaneously with AE monitoring. The experimental samples of sandstone contained electrical resistance strain gauges that monitored full strain data responses during the loading condition. The axial strain data was used solely to produce stress-strain curves for identifying the start of non-linear behavior. The testing area on each specimen received strain gauges through the application of high-strength epoxy resin for the purpose of ensuring accurate measurements. The lead wires underwent a successful curing process to connect them with the digital strain reader through soldering. This monitoring system provides high sensitivity together with resolution capacity that allows users to detect minor strain fluctuations both inside and outside the damage initiation threshold. The UCS loading procedure enabled real-time strain collection, which was then displayed as a stress versus strain relationship. During the first stages of loading, the data points formed a linear pattern, which reflected elastic behavior. The onset of microcracking caused the stress–strain curve to cease its linearity, which enabled researchers to determine the strain at damage initiation. The stress measure obtained at the point of deviation marked the value of σ_{ci}.

4.7 Testing procedures

4.7.1 Macroscopic and Thin Section Analysis of Rock Samples

The examined sandstone specimen features medium to fine grain dimensions while appearing in hand specimens as a reddish-brown rock. The rocks exhibit a high amount of matrix material, which points toward wacke classification. The framework grains of the rock are surrounded by extensive amounts of fine-grained material, which indicates that the rock experienced little sorting during its deposition process. The substantial presence of matrix shows that the rock accumulated within a violent environment with fast deposition, which prevented grain segregation. The rock presents characteristics that match those of wacke sandstones among immature sandstone classifications.

The microscopic examination of sections shows that the rocks cons List of unsorted mixed sand grains that demonstrate coarse psammitic texture. Between 60 μm and 300 μm exist grain dimensions, but the average size measures 150 μm. The sedimentary grains maintain poor sorting patterns while existing mostly as sub-angular to angular types because they experienced limited movement from their proximity to the source area. Approximately 40% of the rock volume consists of a fine-grained matrix that surrounds framework grains in this rock. The facts about the matrix composition are unclear, although its features point toward an origin from clay rocks.

Depth: 36-39 meters

The rock encountered in the depth interval of 36 to 39 meters is primarily a brown, fine-grained, homogeneous, and massive sandstone. The term "massive" indicates a lack of prominent, large-scale internal bedding or structural features within this 3-meter section of the core. The sandstone appears to be texturally uniform with consistent fine grain size distribution throughout. Notably, there are no visible signs of secondary alterations, suggesting the original mineralogical composition and fabric of the sandstone remain largely intact since its deposition and lithification.

However, upon closer examination, the presence of layering is discernible. This layering is not a primary feature of the sandstone matrix itself but is attributed to the alternation of thin layers composed of siltstone, and less frequently, fine-grained sandstone. These interbeds are relatively thin, ranging in thickness from 0.1 to 3.0 centimeters. The orientation of this layering is consistently steeply inclined relative to the core axis, with angles measured between 80 and 85 degrees. Furthermore, the dip azimuth of this layering is 0 degrees, indicating the direction in which these inclined layers would slope downwards if exposed horizontally. This high-angle layering, defined by the intercalation of finer-grained siltstone and occasional slightly coarser sandstone, suggests a history of post-depositional tilting or deformation that has significantly altered the original horizontal orientation of the sedimentary strata.

Depth: 124-128 meters

At a greater depth of 124 to 128 meters, the dominant lithology remains a brown, fine-grained sandstone. However, in contrast to the shallower interval where "massive" was a key descriptor, this deeper section is explicitly described as layered. The primary cause of this distinct layering is the presence of numerous thin interbeds of siltstone, with individual layer thicknesses ranging from 0.1 to 0.5 centimeters. These siltstone layers represent finer-grained depositional events within the overall sandstone sequence.

In addition to the dominant siltstone interbeds, there are also subordinate layers of fine-grained, grayish-brown sandstone. These sandstone layers exhibit a greater variability in thickness, ranging from 0.1 to 5.0 centimeters. This indicates some degree of heterogeneity within the sandstone itself at this depth, with slightly coarser or compositionally distinct sandstone units interbedded with the finer-grained material and the siltstone layers.

Similar to the shallower interval, the layering in this deeper section is also steeply oriented relative to the core axis, with measured angles ranging from 85 to 90 degrees. This consistent high-angle orientation of the layering at both depths suggests a regional structural control affecting the entire rock mass encountered in the borehole. The layering at this depth is more pronounced and explicitly defines the rock mass character compared to the shallower section where it was a feature within an otherwise massive sandstone. The presence of both siltstone and slightly different sandstone layers contributes to a more heterogeneous and structurally defined rock mass at this deeper interval.

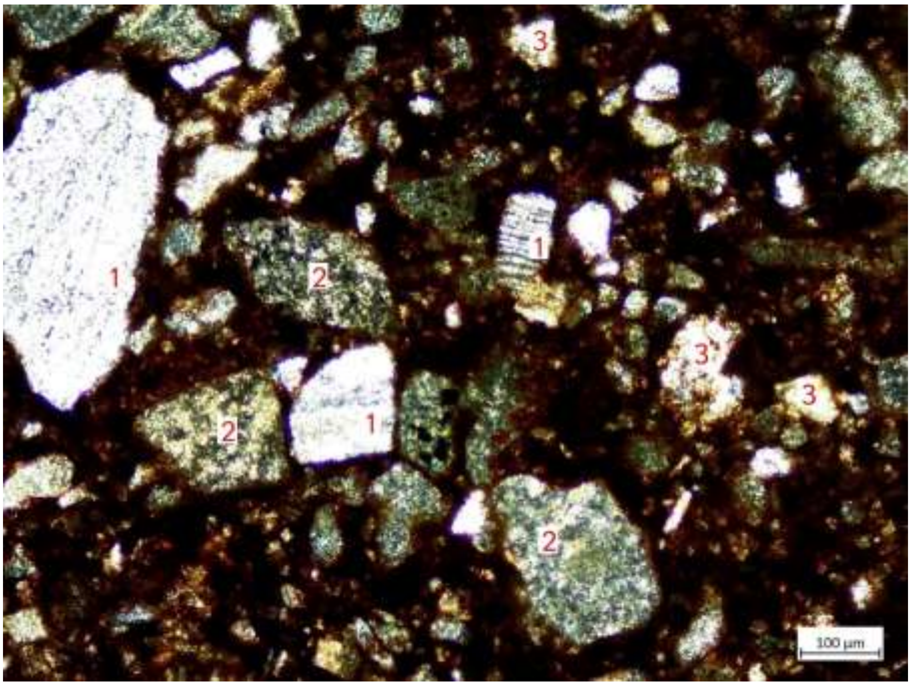

Figure 4.5 XPL of Fe oxidized coarse-grained sandstone weak weathered 1 - Plagioclase, 2 - Quartz, 3 - Siliceous rocks.

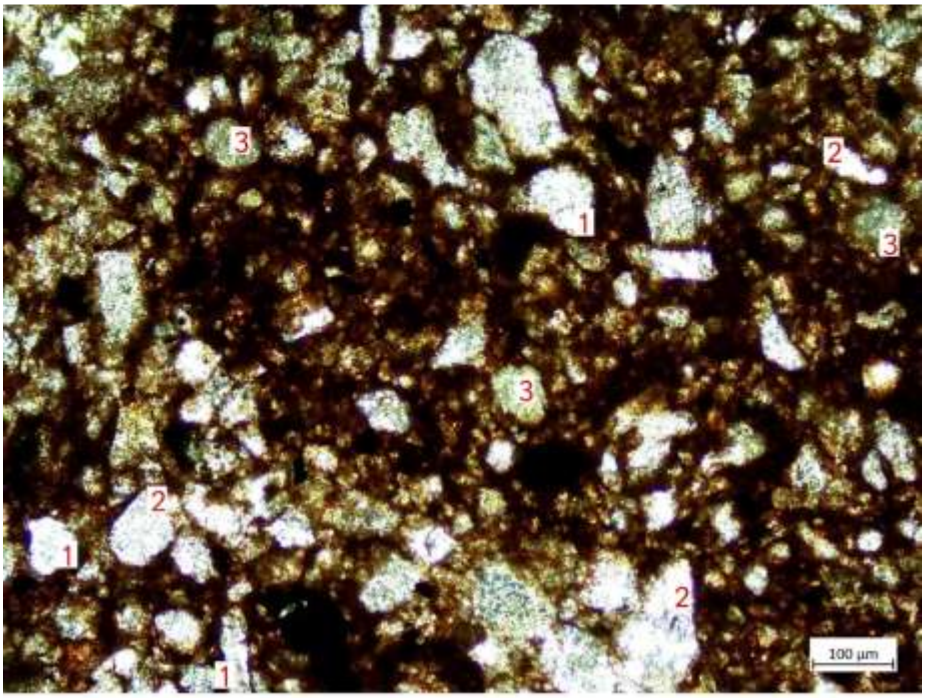

Figure 4.6 XPL of Fe oxidized fine-grained sandstone (siltstone), weak weathered 1 - Plagioclase, 2 - Siliceous rocks, 3 – Quartz

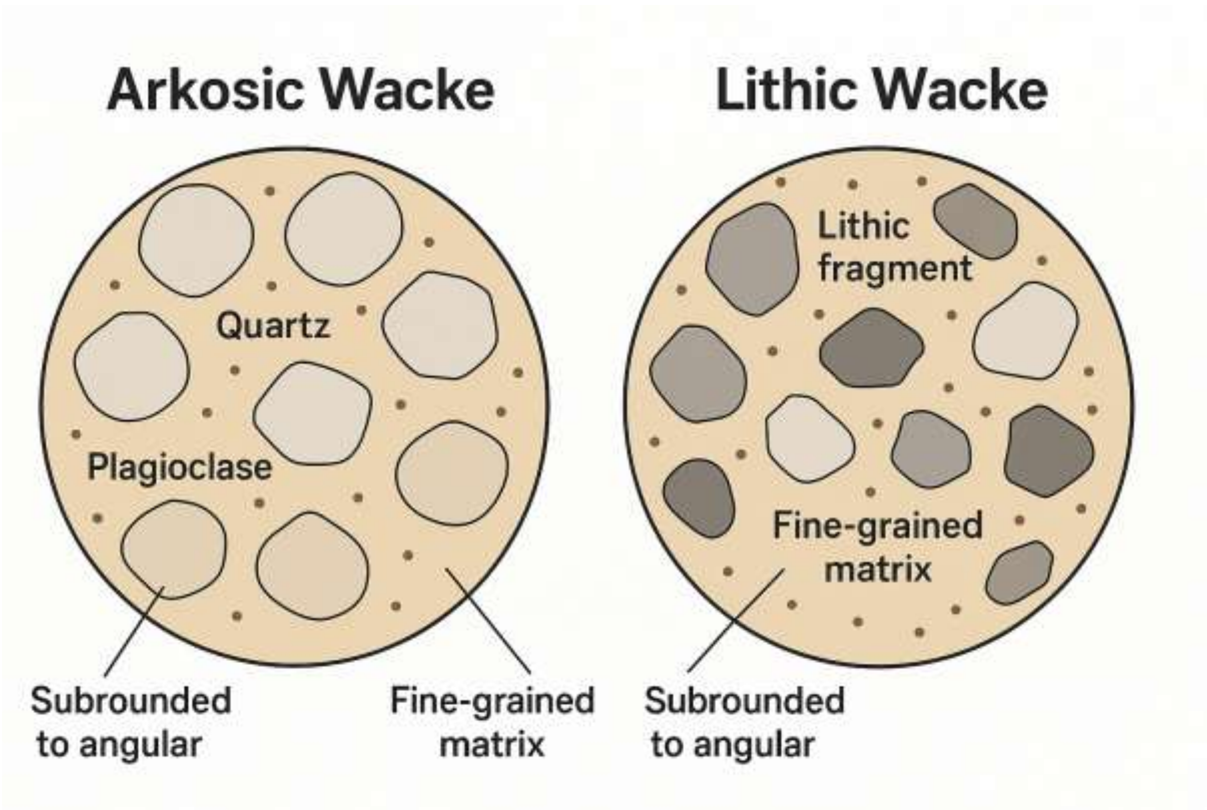

Figure 4. 7 A schematic/thin section-style illustration comparing arkosic vs. lithic wacke

The main mineral elements that comprise the sample consist of quartz and plagioclase feldspar. The presence of plagioclase feldspar becomes apparent when examining the rock specimen under a microscope because feldspar minerals naturally form growth twins. The mix of smaller sub-rounded grains with sizes around 60 μm and larger, more angular clasts that measure 250 μm indicates either multiple sediment sources or varying depositional energy conditions during sedimentation. When viewed under PPL, the cementing material appears brown, which suggests iron oxide. The iron content in this cement helps create the reddish-brown color that appears in the physical rock.

The mechanical behavior of the sandstone samples studied shows a clear dependence on grain size, with coarse-grained samples exhibiting higher strength characteristics compared to fine-grained ones. The uniaxial compressive strength (UCS) values for coarse-grained sandstones such as R1, R4, R5, R6, and R8 average around 134 MPa, while fine-grained samples like R2, R3, R7, R9, and R10 display a lower average UCS of approximately 103 MPa. This suggests that grain size plays a significant role in controlling the rock's overall strength.

Damage initiation stress follows a similar trend. Coarse-grained samples show greater resistance to the onset of internal damage, with average damage stress values around 79 MPa, in contrast to the 38 MPa observed in fine-grained samples. This difference can be attributed to the more interlocked fabric and larger grain contacts in coarse sandstones, which help distribute stress more effectively and delay microcrack formation.

The Hoek-Brown constant 's' further emphasizes this distinction, with coarse-grained sandstones showing higher values (~0.35) and fine-grained ones displaying lower values (~0.13). This aligns with previous studies such as Suorineni et al. (2009), which associate higher 's' values with quartzite or schist-like behavior and lower values with more brittle, granite-like materials. The coarse-grained sandstones appear more ductile and resistant to early fracturing, while the fine-grained samples are more prone to brittle failure.

From a petrographic perspective, these differences reflect the mineralogical and textural maturity of the rocks. The coarse-grained sandstones often show better framework grain interlocking, moderate matrix content, and a dominance of quartz and feldspar, classifying them as arkosic wackes. In contrast, the fine-grained sandstones are more poorly sorted, with higher matrix content and finer textures, consistent with lithic wackes (a relative wacke of which is at least 5% rock fragments, the rock fragments > feldspar, the remainder quartz). The angular grains and high matrix volume suggest rapid deposition, likely in alluvial fan environments.

Ultimately, the combination of petrographic characteristics and mechanical test results shows a strong correlation between grain size, rock fabric, and failure behavior. These findings emphasize the need to consider microstructural and depositional differences when applying failure criteria like Hoek-Brown in sandstone units, especially for design or excavation in variable lithological settings.

The geological classification of this sandstone as arkosic wacke requires feldspar to make up more than 25% of the sample. The sample should be identified as a lithic wacke when lithic fragments occupy significant percentages of the total material. It seems that rapid sedimentation occurred in an alluvial fan or comparable milieu with its poor sorting and angular grains and high matrix content. Sediment burial occurs rapidly in these environments since minimal transport happens, which explains the observed immature texture of sediments.

The occurrence of plagioclase feldspar with growth twins indicates that the rock holds a feldspar-rich mineralogy, which potentially stems from granitic or volcanic geological sources. The combination of rounded smooth grains along with angular clastic fragments exists to demonstrate that deposition took place in a setting characterized by shifting energy levels. Diagenetic changes suggested by iron oxide cement resulted in the reddish-brown visual appearance of the sample. Studies confirm the wacke classification for this sandstone, along with extensive feldspathic origins based on its depositional record and origin.

The first step of thin-section analysis requires technicians to cut small rock sections to 30-micron thickness, which subsequently gets placed on glass slides. Sample preparation utilizes precise milling methods to obtain homogeneous thickness, and a subsequent professional polishing process enhances clarity for microscopes. The preparation process makes sure that mineral grains and textures acquire sufficient visibility for examination purposes. The analysis process revealed all aspects of rock sample composition, including mineral identification and measurement of its size and structure. The identification of minerals and grain sizes enabled researchers to see connections between UCS testing results and these components. The device can inspect numerous substance types, including the polished thin sections researchers used in this research. The combination of energy dispersive morphological information serves to detect minerals present in rock material samples, as shown in Figures 4.8 and 4.9. Here, a sample of coarse-grained almost entirely consists of SiO2 in terms of mass percentage, the chemical composition is: SiO_2 (57.26%), Al_2O_3(14.1%), CaO (2.16%) and MgO (1.99%), while a sample of fine-grained consist of SiO_2 (46.25%), Al_2O_3 (11.92%), CaO (3.4%) and MgO (11.71%).

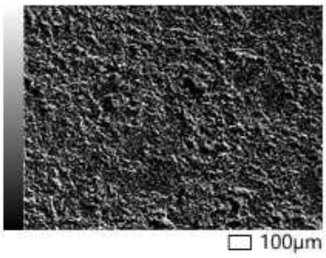

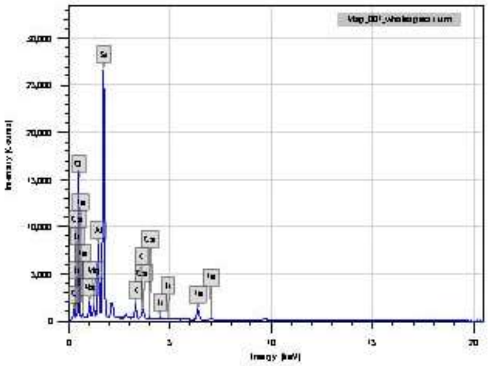

Chemical	Line	Mass%	Mol%	Cations
C	K	11.87±0.	42.23±0.	0.00
O	K			
Na2O	K	3.53±0.0	2.43±0.0	1.06
MgO	K	1.99±0.0	2.11±0.0	0.46
Al2O3	K	14.10±0.	5.91±0.0	2.56
SiO2	K	57.26±0.	40.72±0.	8.84
K2O	K	2.96±0.0	1.34±0.0	0.58
CaO	K	2.16±0.0	1.65±0.0	0.36
TiO2	K	0.50±0.0	0.27±0.0	0.06
FeO	K	5.63±0.0	3.35±0.0	0.73
Total		100.00	100.00	
Map_001_wholespect			Fitting ratio 0.0544	

Figure 4.8 Thin sections, petrographic analysis of coarse-grained, by using SEM

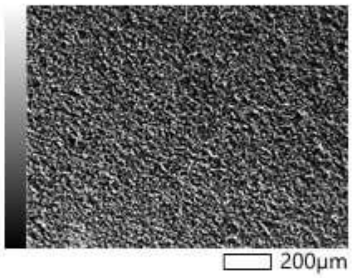

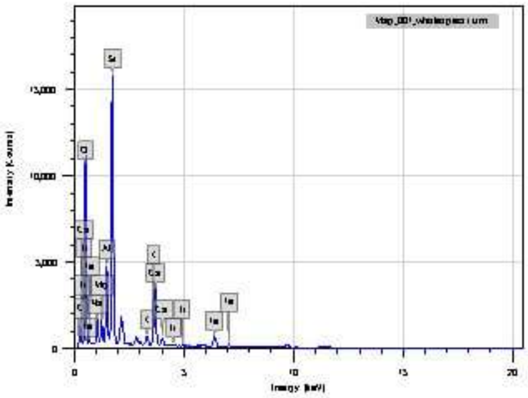

Chemical	Line	Mass%	Mol%	Cations
C	K	16.31±0.	50.54±0.	0.00
O	K			
Na2O	K	4.20±0.0	2.52±0.0	1.39
MgO	K	3.40±0.0	3.14±0.0	0.87
Al2O3	K	11.92±0.	4.35±0.0	2.40
SiO2	K	46.25±0.	28.65±0.	7.90
K2O	K	1.37±0.0	0.54±0.0	0.30
CaO	K	11.71±0.	7.77±0.0	2.14
TiO2	K	0.58±0.0	0.27±0.0	0.07
FeO	K	4.26±0.0	2.21±0.0	0.61
Total		100.00	100.00	
Map_001_wholespect			Fitting ratio 0.0637	

Figure 4.9 Thin sections, petrographic analysis of fine grained by using SEM

5. RESULTS

5.1 Experimental results

In the previous part, it provided a complete explanation regarding the selection of laboratory equipment and experimental setup carried out to test the failure of rock employing UCS testing and Acoustic Emission methodology. The findings will be provided in the following section.

We conducted uniaxial compression tests using GCTS testing system, UCT-1000 testing equipment with cylindric samples, having the load capacity of 1000 kN. In the test, all the collected data was of UCS and acoustic emission data. The testing results showed that the samples were at different stages of the progressive breakdown of the rock.

These yields are, moreover, provided by the sound waves released during deformation and failure of the specimens as proposed by Miao et al. (2021), Zhao & Wen (2018), Eberhardt et al. (1998) and Ghasemi et al. (2020). Sound wave emission data were used to give specific insights about the propagation of cracks.

For each rock sample, ci and the brittle parameter s of Hoek-Brown were estimated for each rock sample. The foregoing characteristics are important in the process of brittle rock fracture. Secondly, the test results showed large difference of the properties of the acquired acoustic events across the loading history, especially before and after the fracture.

To the current study, 10 samples were subjected to uniaxial compression. The stress at which the damage initiation occurs was then deduced. There was initially proposed an innovation of strain gauges incorporation into the study in order to quantify both axial and radial displacement. However, the experimental technique coupled with general equipment used for this study was considered not sufficiently compatible with the given rock samples as evidenced by the time constraints, suboptimal outcomes of the equipment used in combination with other equipment, and it also proved to be not suitable equipment available to use in terms of gauge placement for a number of the available experimental test designs.

Thus, the most appropriate method to measure displacement was to use the GCTS testing machine instead of the strain gauges. Finally, 10 samples were tested with the UCS testing machine. Hoek and Brown (1980) have shown that UCS decreases with increasing specimen diameter but suggested an equation (Eq. 5.1) for converting the value of strength obtained from any specimen other than 63 mm diameter.

$$\frac{UCS}{UCS_{D63}} = \left(\frac{63}{D}\right)^{0.18} \tag{5.1}$$

Table 5.1 shows the UCS converted values for each sample in terms of and according to their corresponding parameters.

Table 5. 1 UCS testing results

Sample	Rock type	Well №	Depth (m)	Diameter (mm)	Height (mm)	Area (mm^2)	UCS (MPa)
R1, R4, R5, R6, and R8	Coarse-grained sandstones Fe oxidized fine-grained sandstone (siltstone), weak weathered	R004	124-128	63	126	7938	103.7 - 152.6
R2, R3, R7, R9, and R10	Fine-grained sandstones (siltstone) Fe oxidized fine-grained sandstone (siltstone), weak weathered	R004	36-39	63	126	7938	73.9 - 124.1

Each sample was calculated for the Young's modulus. The calculation can be done by using any one of several methods used in accepted engineering practice. As measured, it is the proportion of the ultimate strength at some fixed percentage (Figure 5.1 a). It is normally applied at a stress level equal to 50 percent of uniaxial ultimate compressive strength. Another possibility is that the Average Young's modulus is calculated from the average slope of an approximate straight-line portion of the axial stress-axial strain curve (Figure 5.1 b). In this thesis second method was used for the majority of the samples, except in cases where the straight line was not clearly seen, the first method was used.

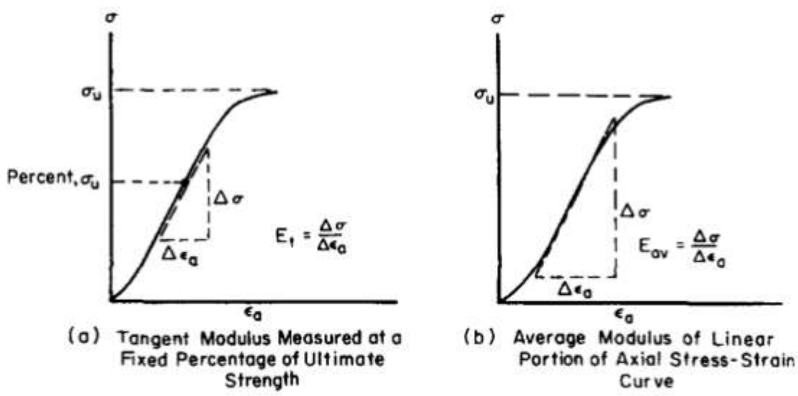

Figure 5. 1 Methods of calculating Young's modulus from axial stress-strain curve (ISRM, 1979)

The relationship between stress (UCS) and strain was graphed. The formula to find Young’s modulus:

$$E = \frac{\Delta\sigma}{\Delta\varepsilon} \tag{5.2}$$

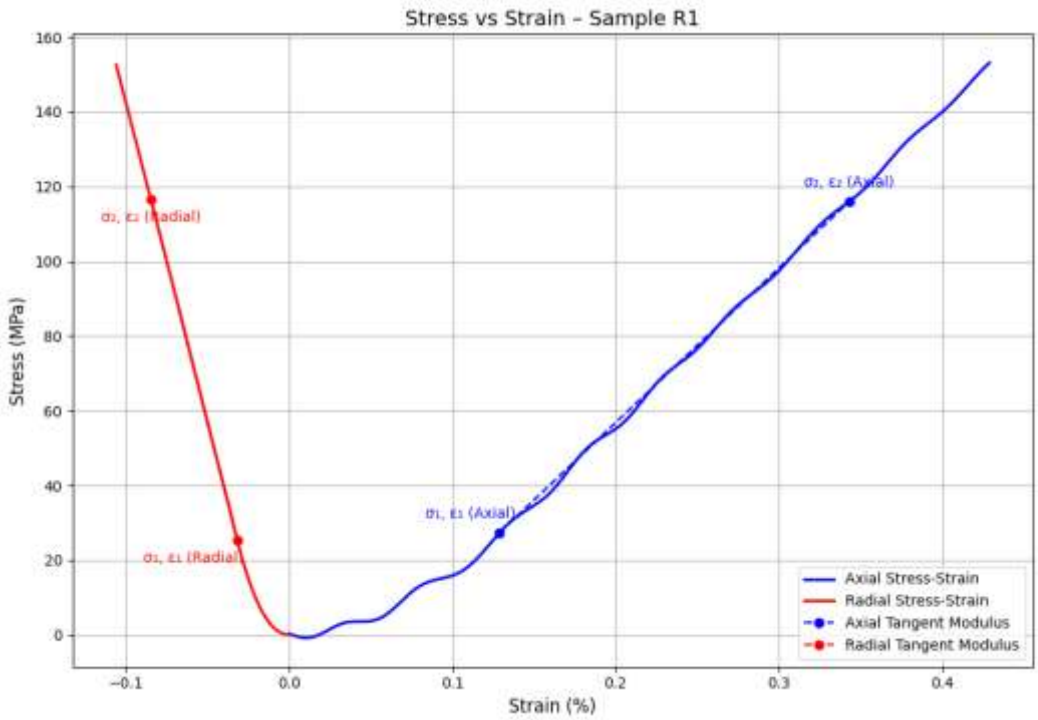

Figure 5. 2 Stress vs strain (R1)

The Young’s modulus (E_t) for the sample:

$$E = \frac{122.08 - 45.778}{0.1287 - 0.3432} = 35{,}57GPa$$

For all specimens, the same methodology is used. The graphs depicted in Figures 5.4 – 5.12, found in Appendix A, and what is described in Table 5.2, are also shown here.

The measurement of Young’s modulus served as a crucial step to understand the elastic properties of sandstone materials during uniaxial compression tests. Compression testing provided strain measurements that enabled researchers to calculate the Young’s modulus (E) to evaluate rock stiffness through strain levels under applied stress. The measurement of sample deformation was possible through strain gauge devices, while researchers derived their conclusions from the slope values found in the linear section of stress–strain data. The strain measurements yielded important information about rock material performance, particularly during evaluations of various grain sizes and rock types. The measured Young's modulus proved valuable for distinguishing between rock samples with different grain sizes because it indicated their respective mechanical properties. Coarse-grained sediment displayed higher elastic modulus readings because such materials demonstrated better stiffness that restricted their elastic behavior. The experimental results served with UCS measurements and Hoek-Brown parameters and damage initiation stress values to gain insight into rock failure behavior. The modulus data formed an integral part of understanding how grain size and matrix distribution influence sandstone mechanical stability during engineering applications.

Using the approach described Suorineni et al., (2009) the damage initiation stress was evaluated based on the UCS and AE values that were obtained. This is based on methodology established the acoustic events are represented by the x-axis and the total axial tension is the y axis. Straight lines connecting the data points on each graph were used to form the curve, through which a smooth curve was fitted. Afterwards, fractures where they manifest and tangents where the first acoustic emission event occurs are delineated using tangents. The two tangents form a junction from which the damage start stress threshold is determined. All specimens were subjected to the specified methodology and the graphical representation of the sample 8 presented above is one of the example cases.

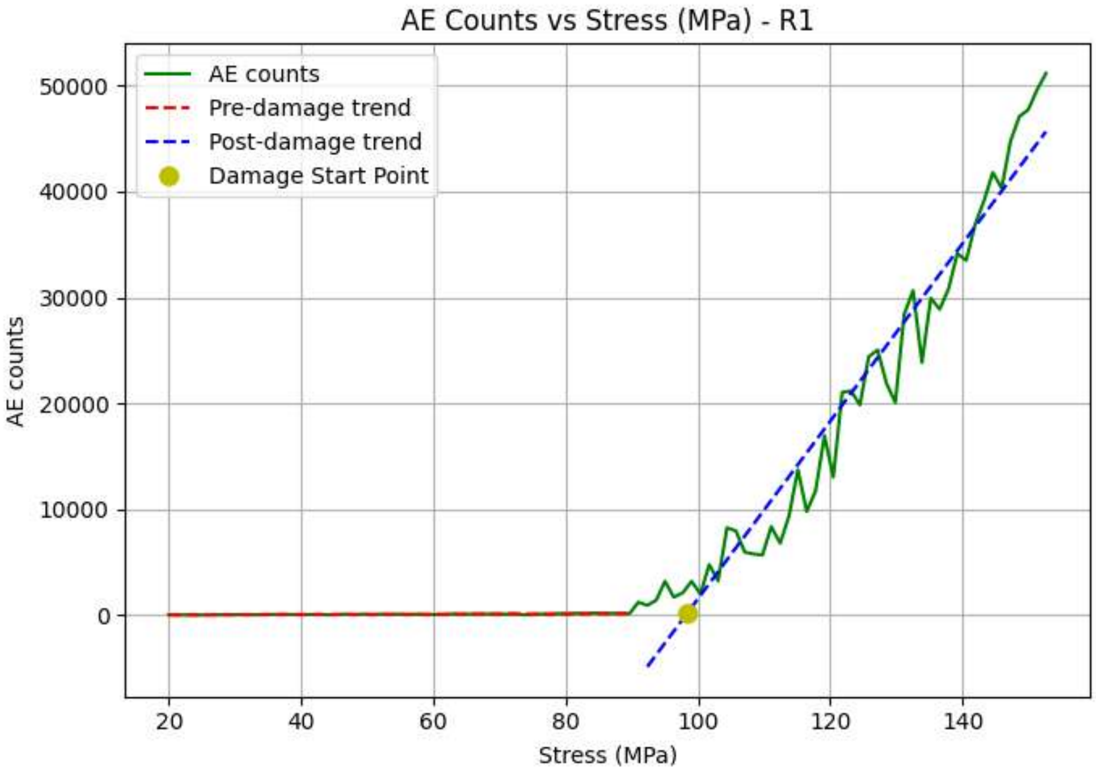

Figure 5. 3 Cumulative AE counts vs UCS graph (R1)

The damage initiation stress threshold (σci) refers to the stress level at which damage begins to occur when the rock is exposed to compressive stress. As the figure shows, for the given sample, the damage initiation stress is approximately equal to 90,034 MPa.

One of the main goals of this research is to determine the brittle Hoek-Brown parameter, s for certain rock types. This aim is achieved by using the modified m-zero initiation criterion proposed by Suorineni et al. (2009) .

In this research, the critical stress is incorporated into Equation 5.3 to get the following equation:

$$\frac{\sigma_{ci}}{\sigma_c} = \mathrm{A} \tag{5.3}$$

Here, A is a constant and it is also defined as

$$\mathrm{A} = \sqrt{s} \tag{5.4}$$

The constant variable A is influenced by the properties of parameter *s* and is also associated with other aspects of a rock's mineralogical composition, texture (such as grain size and shape), foliation, previous stress history, sample disturbance, and metal content.

The s parameter for coarse-grained sandstones composition is derived by using the provided equations and utilizing the findings obtained from testing sample R1.

$$A = \sqrt{s} = \frac{90{,}034}{152{,}6} = 0{,}59$$

$$\mathrm{s} = 0.59^2 = 0.3481$$

The same methodology is used for all specimens. Figures 28-36 depict the graphs, as shown in Appendix A. The analysis dismissed several samples based on their inadequate findings. The findings are shown in Table 5.2 provided below.

Table 5.2 Summary of the results of the tested rocks for the brittle Hoek-Brown constant *s*

Sample ID	Grain Size	Strain gauges (με)	UCS (MPa)	Damage Initiation Stress (MPa)	Young's modulus (GPa)	Poisson's Ratio	Brittle Hoek-Brown Constant $s=(\sigma_{ci}/\sigma_c)^2$
R1	Coarse	921	152,6	90,034	35.57	0.143	0.3481
R2	Fine	714	89,2	35,68	25.67	0.089	0.16
R3	Fine	637	73,9	27,343	23.16	0.075	0.1369
R4	Coarse	855	122,2	69,654	30.85	0.117	0.3249
R5	Coarse	919	152,6	93,086	31.20	0.066	0.3721
R6	Coarse	837	103,7	59,109	27.75	0.091	0.3249

R7	Fine	794	122,3	47,697	30.35	0.092	0.1521
R8	Coarse	854	140,3	84,18	32.25	0.094	0.36
R9	Fine	741	124,1	40,953	30.54	0.092	0.1089
R10	Fine	721	113,8	44,382	29.10	0.093	0.1521

Table 5.3 Sorted results with average s value

Sample	Rock type	Young's modulus (GPa)	UCS (MPa)	Damage Initiation Stress (MPa)	s	Avg s
R1	Coarse	35.57	152,6	90,034	0.3481	
R5	Coarse	31.20	152,6	93,086	0.3721	0,36
R8	Coarse	32.25	140,3	84,18	0.36	
R7	Fine	30.35	122,3	47,697	0.1521	0,1521
R10	Fine	29.10	113,8	44,382	0.1521	

The tested sandstones followed a strength pattern where coarse-grained examples demonstrated higher numbers between 103.7 MPa to 152.6 MPa than the fine-grained type with a range of 73.9 MPa to 124.1 MPa, as it is shown in Table 5.2. Strain gauge data showed coarse-grained samples reaching higher strain measurements of 919 $\mu\varepsilon$ as peak values on Sample R5 compared to the maximal strain of 794 $\mu\varepsilon$ in fine-grained samples on Sample R7. The point of linear elasticity deviation occurs at higher damage initiation stress levels in fine-grained sandstones with strong cementation in Samples R9 (124.1 MPa) and R7 (122.3 MPa). The UCS values of certain coarser sandstones displaced damage earlier than one would expect because their heterogeneous structure and pore features resulted in earlier onset of damage according to tests on Samples R6 (103.7 MPa) and R4 (122.2 MPa).

All ten of these sandstone samples have stress–strain profiles that evolve from elastic to plastic deformation in a similar fashion for increasing load. All the curves feature a single linear elastic region and a deviation, which is due to the start of micro-crack propagation. High UCS values (122.2 MPa − 152.6 MPa) and relatively high σ_{ci} ($\geq$ 69.7 MPa) were observed for samples R1, R4, R5, and R8, resulting in strain at crack initiation, for all cases exceeding 480 $\mu\varepsilon$. Features such as this indicate a strong interlocked grain structure of such extent as to withstand stress and resist premature damage. The stress–strain curves seem to be very long in linearity, suggesting resilient cohesion and, thus, resistance to the early micro-crack appearance. Instead, the samples R2, R3, R9, and R10 (as a representative of finer-grained sandstone) showed much higher UCS as well as much earlier damage initiation. The most brittle R3 σci = 27.3 MPa, failed under a minimum of microstructural disturbance. These samples are early, therefore suggesting the low capacity to redistribute stress, possibly due to internal flaws, finer grain contact, or cementation characteristics. For samples R6 and R7, the UCSs (103 MPa −122 MPa) and σci (47.7 MPa − 59.1 MPa) were moderate. Their curves would imply a balance of structural resistance against microcrack initiation or heterogeneity in grain size or bonding. There is a group of these transitional cases that fill the mechanical gap between the more ductile, coarse-grained sandstones and the more brittle, fine-grained sandstones.

Results from silica-cemented sandstones show a strong relationship exists between grain size and mechanical qualities. The mechanical properties of silica sandstones reached higher levels in specimens with fine-grained sand (grain size <0.25 mm) than specimens having coarse-grained sand (grain size >0.5 mm). The enhanced interlocking effect between grains and uniform cementation makes fine-grained varieties exhibit stronger mechanical properties. The rock mass strength increases according to the Hoek-Brown failure criterion because of its enhanced "s" parameter. The strength potential of coarse-grained silica sandstones tends to decrease because the structure contains both patchy cementation and grain-supported characteristics that limit the effectiveness of grain-to-grain contact behavior. Acoustic emissions responded differently between the two types of sandstone throughout the laboratory testing. The failure process of fine-grained sandstones occurred through gradual acoustic emission signals that revealed a smoother mode of failure. Brittle failure occurred within coarse-grained sandstones because they produced strong acoustic emission signals that were abrupt and sharp. Research findings establish that the mechanical properties of silica-cemented sandstones heavily depend on their grain size characteristics.

The values of damage initiation stress offer extra information about the mechanical response of these sandstones. The coarse-grained samples demonstrate higher UCS values (103.7 – 152.6 MPa) as well as elevated damage initiation stress values because they require greater applied loads before developing microfracture propagation. The measured s values for these sandstone samples show minimal variations compared to the values reported in Suorineni et al. (2009) for granitic rock samples, which indicates identical failure responses. Although fine-grained sandstones display lower strength levels, their damage initiation stress occurs earlier under conditions that affect quartzite and granodiorite rocks. According to Suorineni et al.'s (2009) depth-of-failure model, an incorrect estimation of s value in fine-grained sandstones produces excessive failure depth estimates, thus creating designs that use too many safety factors. When the cohesion of coarse-grained samples is overestimated, the actual failure depth becomes underestimated, which results in unsafe excavation conditions. A refinement of the Hoek-Brown s parameter based on rock composition is essential to achieve better accuracy in geomechanically stability evaluations.

The lithology and grain size affected the intact rock material strength characteristics based on the criterion of this definition since the variation of '*s*' across a variety of rock types and within the sandstone samples exhibits a clear trend. However, Suorineni et al. 2009 data shows a range of 's' values, of which the granite has the lower 's' (0.16), and quartzite higher 0.21-0.36 's'. The 's' value is found to be correlated to a particular grain size for the sandstone samples. R1, R5, and R8 have higher 's' value averages (0.36), which is analogous to quartzite as well as schist. Such a lesion to the fabric has resulted in larger grain size in these sandstones, which contribute to higher resistance to initial failure because of more interlocked fabric. Unlike the fine-grained samples (R7, R10), the average s value is lower on these samples (0.15), which are similar to granite and some schist varieties. This finer internal structure likely leads to a different failure mechanism under stress. Therefore, the critical role of the grain size in the Hoek Brown framework's intact material constants '*s*' is brought into a sharp focus with the coarser grains linked to higher '*s*' values and finer grains associated with lower 's' values and different intact rock materials behavior.

The observed differences in rock behavior can be attributed to the variations in grain size and its influence on stress distribution and crack propagation within the rock's microstructure. Coarse-grained rocks, characterized by larger mineral particles, tend to distribute stress concentrations at grain-to-grain contacts. This interlocking structure contributes to their higher strength and resistance to damage initiation, as more energy is required to initiate and propagate cracks through the larger grains or along their boundaries. Conversely, fine-grained rocks possess a greater grain boundary area, providing more surfaces where crack initiation and propagation can occur. This inherent structural characteristic leads to lower strength and a propensity for damage to initiate at lower stress levels.

Laboratory tests established that compressive failure mechanics of sandstone materials differs substantially between fine- and coarse-grained components due to their different Hoek-Brown *s* constant values. The s values for coarse-grained sandstones extend between 0.32 to 0.37 and fine-grained sandstones display lower s ranges from 0.11 to 0.16 as shown in Table

5.2. Research conducted by Suorineni et al. (2009) confirms that rock types have distinct s parameters, as observed in this study. The wide range of s values shows why it is not correct for all types of rock to use the s = 0.11 cohesion constant of the brittle Hoek-Brown criterion. The widely applied cohesive parameter, however, leads to large discrepancies when the excavation damage is estimated and, in particular, for rocks having high and low values of cohesion naturally. The default value of s = 0.11 would produce underestimations in damage assessments for our fine-grained specimens R2, R3, R9, and R10 because they exhibit cohesion levels significantly exceeding this assumption.

A clear trend emerges from the data: coarse-grained rock samples tend to exhibit higher UCS values and higher damage initiation stress levels compared to fine-grained samples. This indicates that coarse-grained rocks are generally stronger and more resistant to the onset of internal damage. Samples R1, R4, R5, R6, and R8, all classified as coarse-grained, demonstrate higher strength and a greater capacity to withstand stress before damage initiation. In contrast, fine-grained samples R2, R3, R7, R9, and R10 show a pattern of lower UCS and damage initiation stress, suggesting a lower resistance to both overall failure and the initiation of internal damage.

Table 5. 4 Summary of the results of the tested rocks for the brittle Hoek-Brown constant *s* between 2002 and 2009 (Suorineni et al. 2009)

Rock type	**Brittle Hoek-Brown Constant *s***
Granite	0.16
Granodiorite	0.53
Diorite	0.53
Norite	0.42
Quartzite 1	0.36
Quartzite 2	0.28
Quartzite 3	0.21
Schist 1	0.36
Schist 2	0.25
Schist 3	0.15

In summary, the grain size of a rock plays a crucial role in determining its mechanical behavior under stress. Coarse-grained rocks are generally stronger and more resistant to damage, while fine-grained rocks are weaker and more susceptible to damage initiation at lower stress levels. The Brittle Hoek-Brown Constant '*s*' effectively captures this relationship, reflecting the proportion of rock strength utilized before the onset of significant damage and highlighting the importance of considering grain size in rock mechanics analyses and engineering applications.

6. CONCLUSIONS AND RECOMMENDATIONS

The goal of this work highlighted an investigation of sandstone properties at both the microscopic and macro levels, as well as a study of their mechanical properties using uniaxial compressive strength (UCS) tests and strain gauge methods. Two types of sandstone, namely, fine-grained and coarse-grained, received investigation to identify the variations in their structural elements and mineral content, and mechanical properties. The time of rapid sedimentation becomes evident through thin-section analysis because the sandstone samples contain poorly sorted sub-angular to angular grains that are embedded in fine-grained matrix material. The rock contains an iron oxide cementation that modifies both its cohesion and strength properties among major mineral components of quartz and plagioclase feldspar. The petrographic field observations demonstrated that the analyzed rock represents both arkosic wacke and lithic wacke depending on the presence of major lithic fragments.

Experimental tests using UCS methodology revealed separate failure modes and strength properties between fine-grained and coarse-grained sandstone material types during their deformation tests. The UCS results showed that the stiffness of samples based on grain size distribution with coarse-grained sandstone ranging from 103.7 MPa to 152.6 MPa and fine-grained sandstone measuring from 73.9 MPa to 124.1 MPa. The results from strain gauges showed that fine-grained samples absorbed less strain than coarse-grained samples, which displayed larger strain because grain boundary connections delayed their breakage. A substantial difference existed between the stress deviation onset for fine-grained sandstones, which started before their coarse-grained counterparts did. The results demonstrate how grain size, together with matrix material, influences rock failure processes as well as the strength characteristics and mechanical properties of deformation.

Additional information about sample sandstone cohesion was obtained through the brittle Hoek-Brown s parameter evaluation. When measuring s values for fine-grained sandstone samples, the obtained results are 0.108-0.16, and for coarse-grained samples, the values ranged between 0.324 and 0.372. The measured s values surpass the $s = 0.11$ value used in the original brittle Hoek-Brown criterion, indicating a need for rock type-specific determination of this parameter. The use of a single universal s value for failure depth estimation led to incorrect predictions of excavation damage in fine-grained sandstones because these rocks showed higher cohesion than the initial assumptions. Incorrect assumptions of rock cohesion generate problems with underground excavation stability because they create either too safe or unsafe design parameters. The research demonstrates why petrographic investigation alongside mechanical testing leads to better rock classification, which enhances geomechanically evaluations. These findings demonstrate the inappropriate nature of adopting generalized Hoek-Brown parameters across different rock formations because matrix composition and grain shape vary substantially in their strength effects. Improved mechanical models for rocks of a specific type are needed to enable it to supplement the effectiveness of stability assessments in underground construction in conjunction with petroleum reservoir management strategies.

Recommendations

1. These studies provide hypothetical ideas for enhancing rock strength characterization and excavation stability along with geomechanical modeling which need empirical verification.

2. Results show that numerical variation in the s parameter of brittle Hoek-Brown material exists between diverse sandstones in terms of its grain sizing. Cohesion constants unique to given rock type rather than use of the generalized value of $s = 0.11$ in modelling protocols, are required. Additional experimental testing with various sandstone samples should be performed to build a complete database focused on refining Hoek-Brown failure criteria for sedimentary rock formations.

3. Cross-analysis of rock formations' mechanical stability needs UCS testing and petrographic analysis before implementation by underground excavation engineers and geologists. The predictions should include adjustments using specific s values for each rock type to prevent safety-threatening misestimations. Regular petrographic analysis of thin sections is performed during the GSI testing procedures to better determine how the rock behaves depending on the grain size and sorting pattern, as well as the composition of the matrix. Research should explore mineralogical composition variations to establish quantitative relationships for better rock failure behavior prediction models.

4. Experimental evidence of iron oxide cementation in the analyzed specimens demonstrates that rock diagenesis leads to substantial modifications of cohesive strength properties. Research should evaluate the effects on UCS and failure behavior of sandstones through studies focused on various cementing agents, including silica, carbonate, and iron oxide.

This research uses petrographic analysis together with UCS testing and strain gauge instrumentation to develop an extensive examination of fine- and coarse-grained sandstone mechanical properties. Rock-specific failure criteria demand attention because the study demonstrates their significance together with laboratory methods that combine petrographic microscopy examination and mechanical testing. Geomechanical models will receive better predictions for excavation stability while understanding reservoir rock behavior more precisely through the detailed study and application of Hoek-Brown s parameter as well as petrographic information. The ideas presented here will serve as the basis for future research targeted at maximizing rock strength characterisation and increasing safety in subterranean construction and engineering.

7. REFERENCES

AE Institute Co., Ltd. (2017). SAEU3H AE system User manual. QingCheng. https://www.acousticemission.cn/pro/list921.html

B. H. G., & Brown, E. T. (2006). *Rock mass structure and characterisation.* In *Rock mechanics for underground mining* (3rd ed., pp. 46–84). Springer. https://doi.org/10.1007/978-1-4020-2116-9

Bieniawski, Z., & Bernede, M. (1979). Suggested methods for determining the uniaxial compressive strength and deformability of rock materials. International Journal of Rock Mechanics and Mining Sciences & Geomechanics Abstracts, 16(2), 138–140. https://doi.org/10.1016/0148-9062(79)91451-7

Castro, L. A. M., McCreath, D. R., & Oliver, P. (1996). Rockmass damage initiation around the Sudbury neutrino observatory cavern. In *ARMA North America Rock Mechanics Symposium* (pp. ARMA-96). ARMA. https://onepetro.org/ARMANARMS/proceedings-abstract/NARMS96/All-NARMS96/130805

Cundall, P. A., Potyondy, D. O., & Lee, C. A. (1996). Micromechanics-based models for fracture and breakout around the mine-by tunnel. In *proceedings, international conference on deep geological disposal of radioactive waste, Winnipeg. Edited by JB Martino and CD Martin. Canadian Nuclear Society, Toronto* (pp. 113-122).

Diederichs, M. S., Kaiser, P. K., & Eberhardt, E. (2004). Damage initiation and propagation in hard rock during tunnelling and the influence of near-face stress rotation. *International Journal of Rock Mechanics and Mining Sciences*, *41*(5), 785-812. https://doi.org/10.1016/j.ijrmms.2004.02.003

Eberhardt E (1998) Brittle rock fracture and progressive damage in uniaxial compression. Ph.D. thesis, Department of Geological Sciences, University of Saskatchewan, Saskatoon

Eberhardt, E. B. (1998). *Brittle rock fracture and progressive damage in uniaxial compression* (Doctoral dissertation, University of Saskatchewan). https://harvest.usask.ca/bitstream/10388/etd-10212004-001228/1/NQ27403.pdf

Feng, G., Xia, G., Chen, B., Xiao, Y., & Zhou, R. (2019). A method for rockburst prediction in the deep tunnels of hydropower stations based on the monitored microseismicity and an optimized probabilistic neural network model. *Sustainability, 11(11),* 3212. https://doi.org/10.3390/su11113212

Grimstad, E., & Bhasin, R. (1999). Rock support in hard rock tunnels under high stress. *Publikasjon-Norges Geotekniske Institutt, 205*.

Hoek E., Brown, E.T. (1980). Underground excavations in rock. Institution of Mining and Metallurgy, London, 527 pp. 7.

Hoek, E., Carranza-Torres, C., & Corkum, B. (2002). Hoek-Brown failure criterion—2002 edition. *Proceedings of NARMS-Tac, 1(1),* 267–273.

Hoek, E., Carter, T. G., & Diederichs, M. S. (2013). Quantification of the geological strength index chart. In *ARMA US Rock Mechanics/Geomechanics Symposium* (pp. ARMA-2013). ARMA. https://onepetro.org/ARMAUSRMS/proceedings-abstract/ARMA13/All-ARMA13/121184

Hoek, E., Wood, D., & Shah, S. (1992). A modified Hoek–Brown failure criterion for jointed rock masses. In *Rock Characterization: ISRM Symposium, Eurock'92, Chester, UK, 14–17 September 1992* (pp. 209-214). Thomas Telford Publishing. https://www.icevirtuallibrary.com/doi/pdf/10.1680/rc.35621.0037

Martin, C. D. (1990). Characterizing in situ stress domains at the AECL Underground Research Laboratory. *Canadian Geotechnical Journal*, *27*(5), 631-646. https://cdnsciencepub.com/doi/abs/10.1139/t90-077

Martin, C. D. (1993). The strength of massive Lac du Bonnet granite around underground openings. https://mspace.lib.umanitoba.ca/bitstream/1993/9785/1/Martin_The_strength.pdf

Martin, C. D., Kaiser, P. K., & McCreath, D. R. (1999). Hoek-Brown parameters for predicting the depth of brittle failure around tunnels. *Canadian Geotechnical Journal, 36(1),* 136–151. https://doi.org/10.1139/t98-072

Martini, C. D., Read, R. S., & Martino, J. B. (1997). Observations of brittle failure around a circular test tunnel. *International Journal of Rock Mechanics and Mining Sciences*, *34*(7), 1065-1073. https://doi.org/10.1016/S1365-1609(97)90200-8

Mathews, J. H., Hoek, E., Chandler, E., Redmond, C., & Ozunchu, N. (1990). The determination of geological parameters for the design of slopes in jointed rock. In *Proceedings of the International Symposium on Rock Joints* (pp. 531–545). Balkema.

Mohammed, J. A. (2015). *Underground structures support, stress & strain of tunnel.* ResearchGate. https://doi.org/10.13140/RG.2.2.25253.50400

Mohammed, M., Shafiq, N., Abdallah, N. A. W., Ayoub, M., & Haruna, A. (2020). A review on achieving sustainable construction waste management through application of 3R (reduction, reuse, recycling): A lifecycle approach. *IOP Conference Series: Earth and Environmental Science, 476(1),* 012010. https://doi.org/10.1088/1755-1315/476/1/012010

Palmstrom, A. (2005). Measurements of and correlations between block size and rock quality designation (RQD). *Tunnelling and Underground Space Technology, 20(4),* 362–377. https://doi.org/10.1016/j.tust.2005.01.005

Read, R. S. (1994). Interpreting excavation-induced displacements around a tunnel in highly stressed granite. https://mspace.lib.umanitoba.ca/bitstreams/cb531bc3-eee7-46c9-a60d-65fa15ef0be9/download

Read, R. S. (2004). 20 years of excavation response studies at AECL's Underground Research Laboratory. *International Journal of Rock Mechanics and Mining Sciences*, *41*(8), 1251-1275. https://doi.org/10.1016/j.ijrmms.2004.09.012

Read, S. A. L., & Richards, L. (2015, May). Guidelines for use of tensile data in the calculation of the Hoek-Brown constant mi. In *ISRM Congress* (pp. ISRM-13CONGRESS). ISRM. https://onepetro.org/isrmcongress/proceedings-abstract/CONGRESS13/All-CONGRESS13/165724

Renani, H. R., & Cai, M. (2021). Forty-year review of the Hoek–Brown failure criterion for jointed rock masses. *Rock Mechanics and Rock Engineering, 55(1),* 439–461. https://doi.org/10.1007/s00603-021-02661-2

Suorineni, F. T., & Kaiser, P. K. (2002). Characteristic acoustic properties of sulphide ores and host rocks. In Hammah, R., Bawden, W. F., Curran, J., & Telsnicki, M. (Eds.), *Proceedings of the 5th North American Rock Mechanics Symposium (NARMS),* Toronto, Canada (pp. 403–410). University of Toronto Press.

Suorineni, F. T., Chinnasane, D. R., & Kaiser, P. K. (2009). A procedure for determining rock-type specific Hoek-Brown brittle parameter *s. Rock Mechanics and Rock Engineering, 42(6),* 849–881. https://doi.org/10.1007/s00603-008-0024-y

Ulusay, R. (Ed.). (2015). *The ISRM suggested methods for rock characterization, testing and monitoring: 2007–2014.* Springer. https://doi.org/10.1007/978-3-319-07713-0_1

Wagner, H. (1987). Design, support of underground excavations in highly stressed rock. In *Proceedings of the 6th ISRM Congress*, Montreal, Canada (pp. 1443–1457). https://cir.nii.ac.jp/crid/1573387448889082880

Zhang, J. (2018). Investigation of relation between fracture scale and acoustic emission time-frequency parameters in rocks. Shock and Vibration, 2018, 1-14. https://doi.org/10.1155/2018/3057628

Zhang, K., Zhang, S., Ren, J., Wang, M., Shuai, J., & Zhang, W. (2023). Study on characteristics of acoustic emission b value of coal rock with outburst-proneness under coupled static and dynamic loads. Shock and Vibration, 2023, 1-13. https://doi.org/10.1155/2023/2400632

Zhao, X., Deng, L., & Xu, J. (2020). Defining stress thresholds of granite failure process based on acoustic emission activity parameters. Shock and Vibration, 2020, 1-8. https://doi.org/10.1155/2020/8812066

8. APPENDICES

8.1 Appendix A

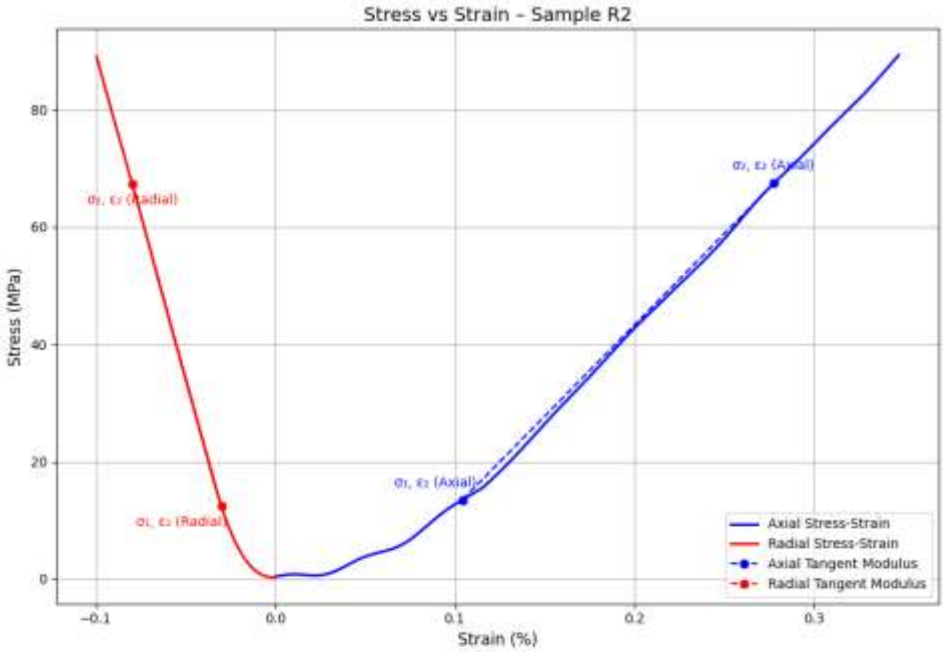

Figure 5.4 Stress vs strain (R2)

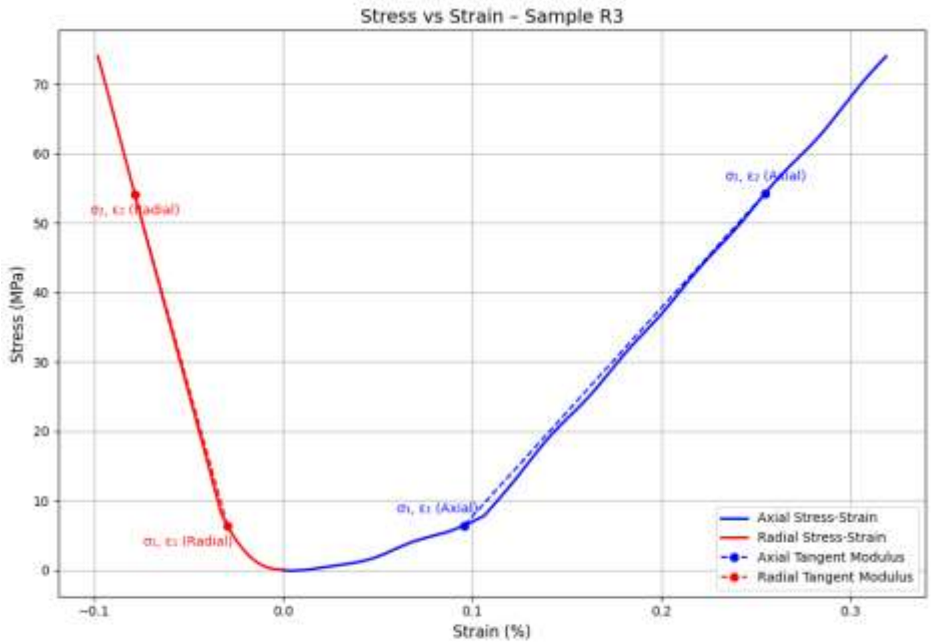

Figure 5.5 Stress vs strain (R3)

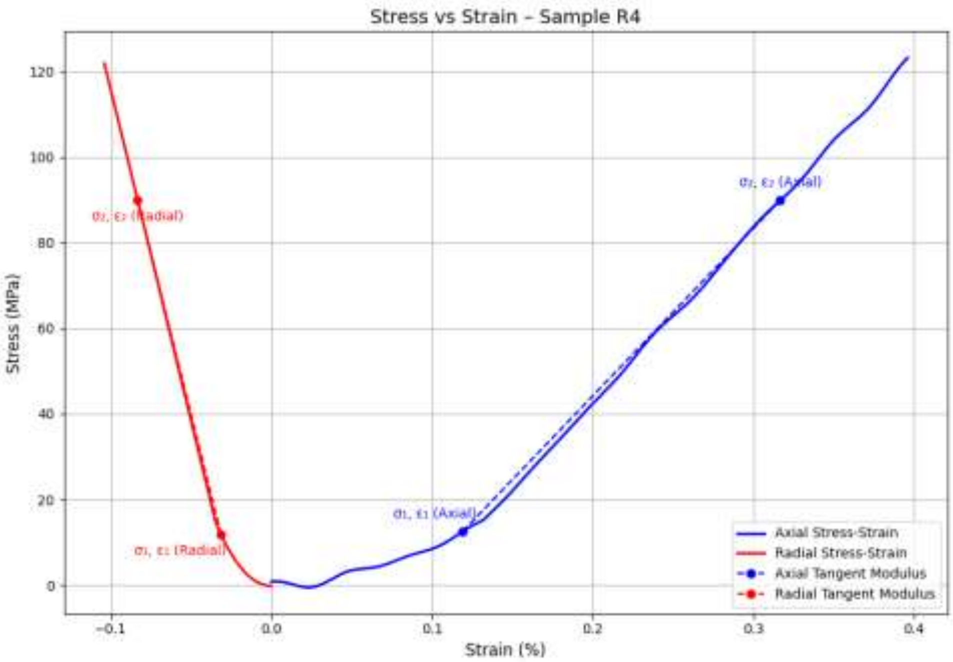

Figure 5.6 Stress vs strain (R4)

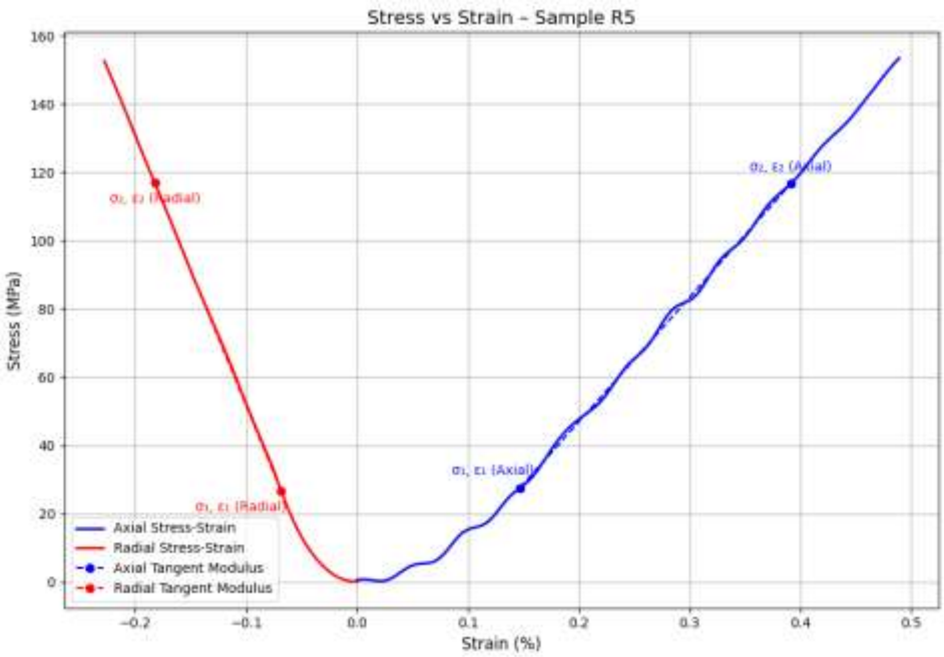

Figure 5.7 Stress vs strain (R5)

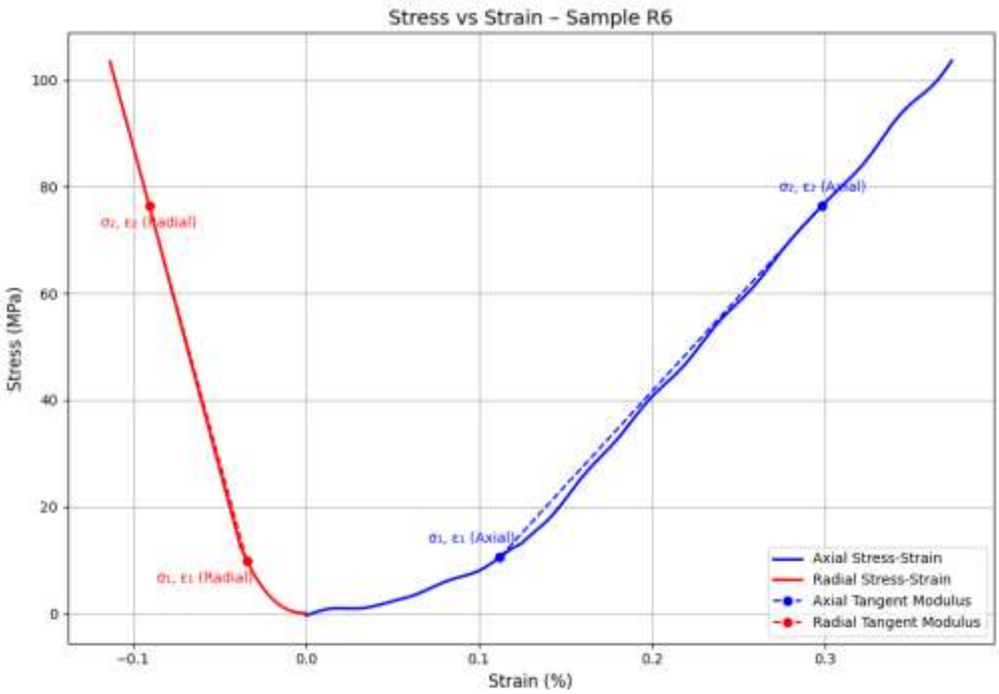

Figure 5.8 Stress vs strain (R6)

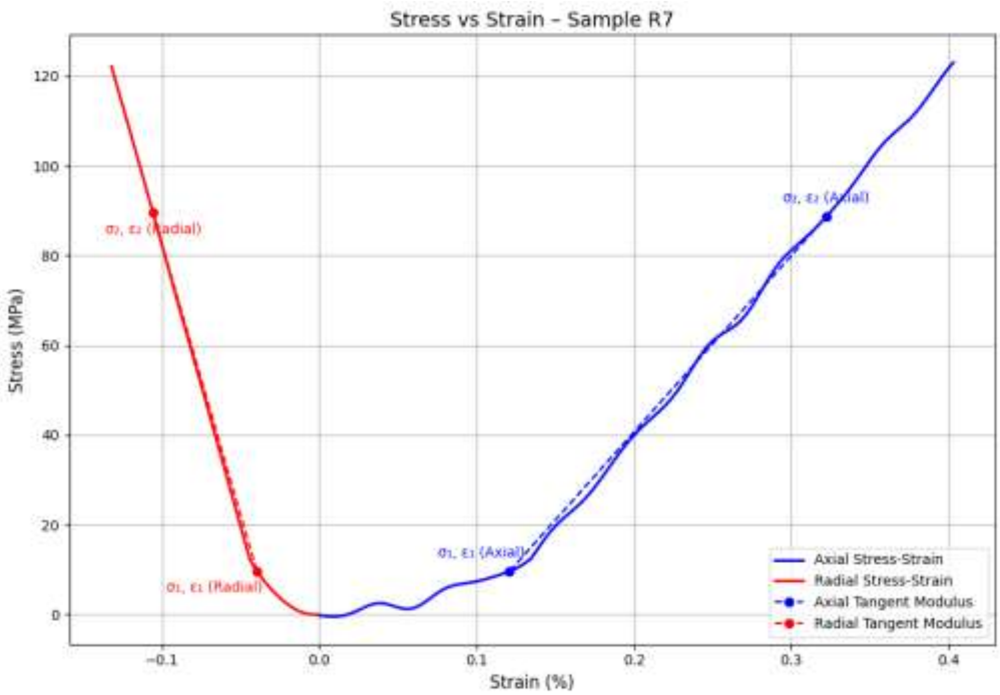

Figure 5.9 Stress vs strain (R7)

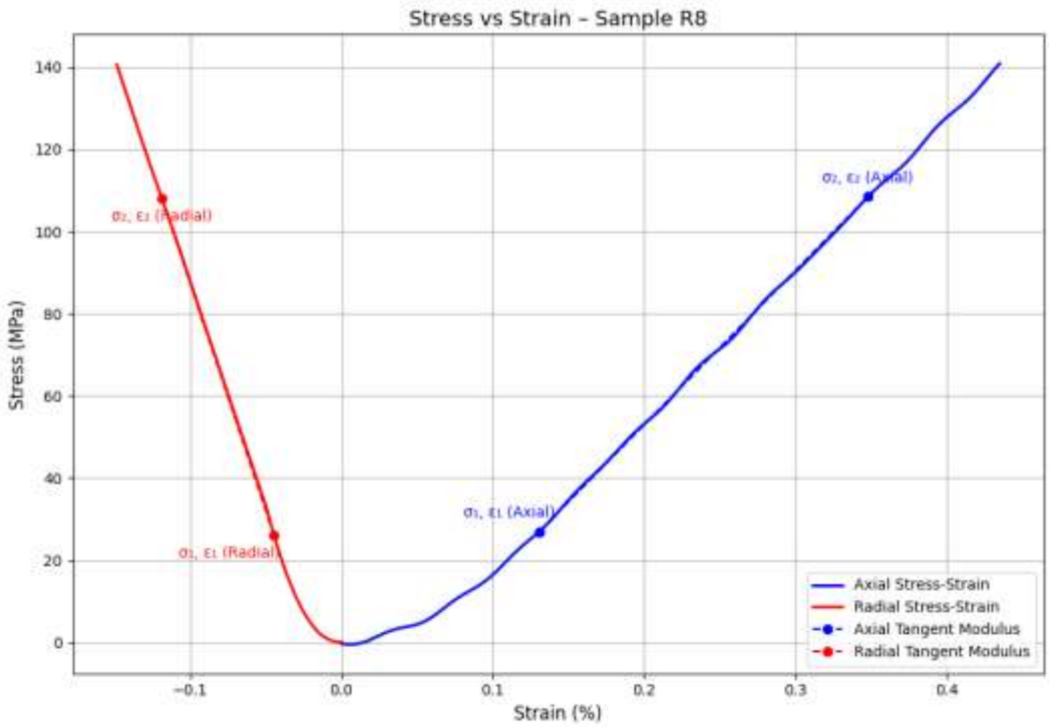

Figure 5.10 Stress vs strain (R8)

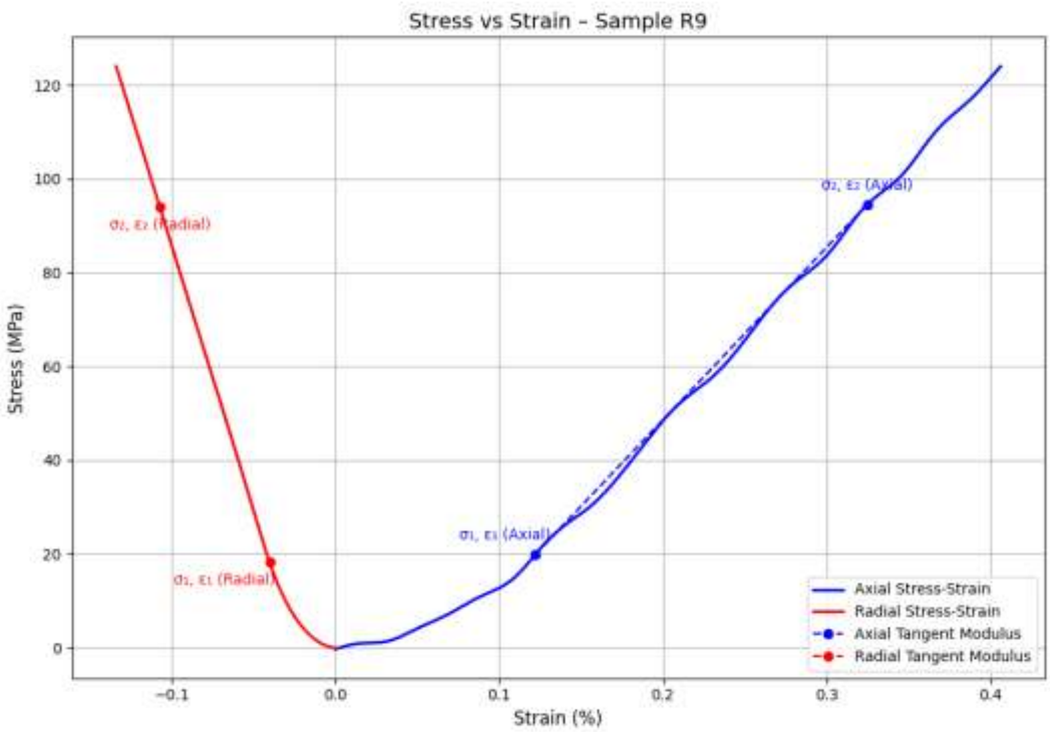

Figure 5.11 Stress vs strain (R9)

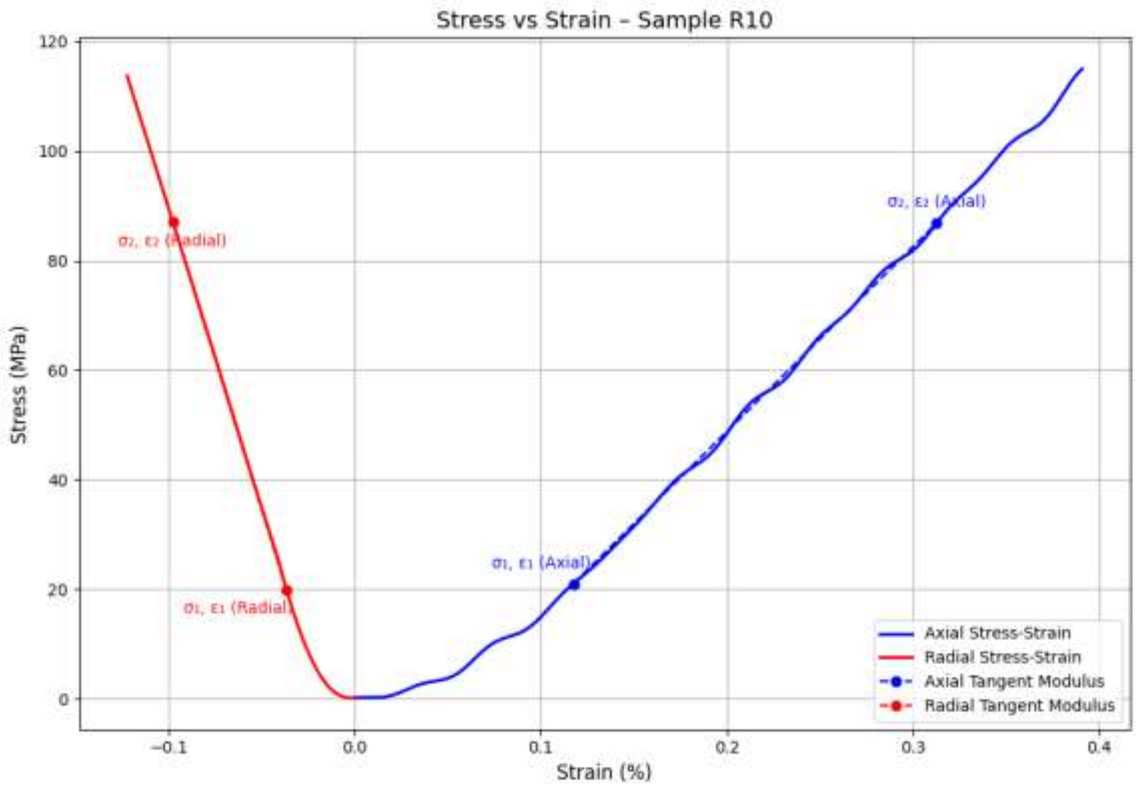

Figure 5.12 Stress vs strain (R10)

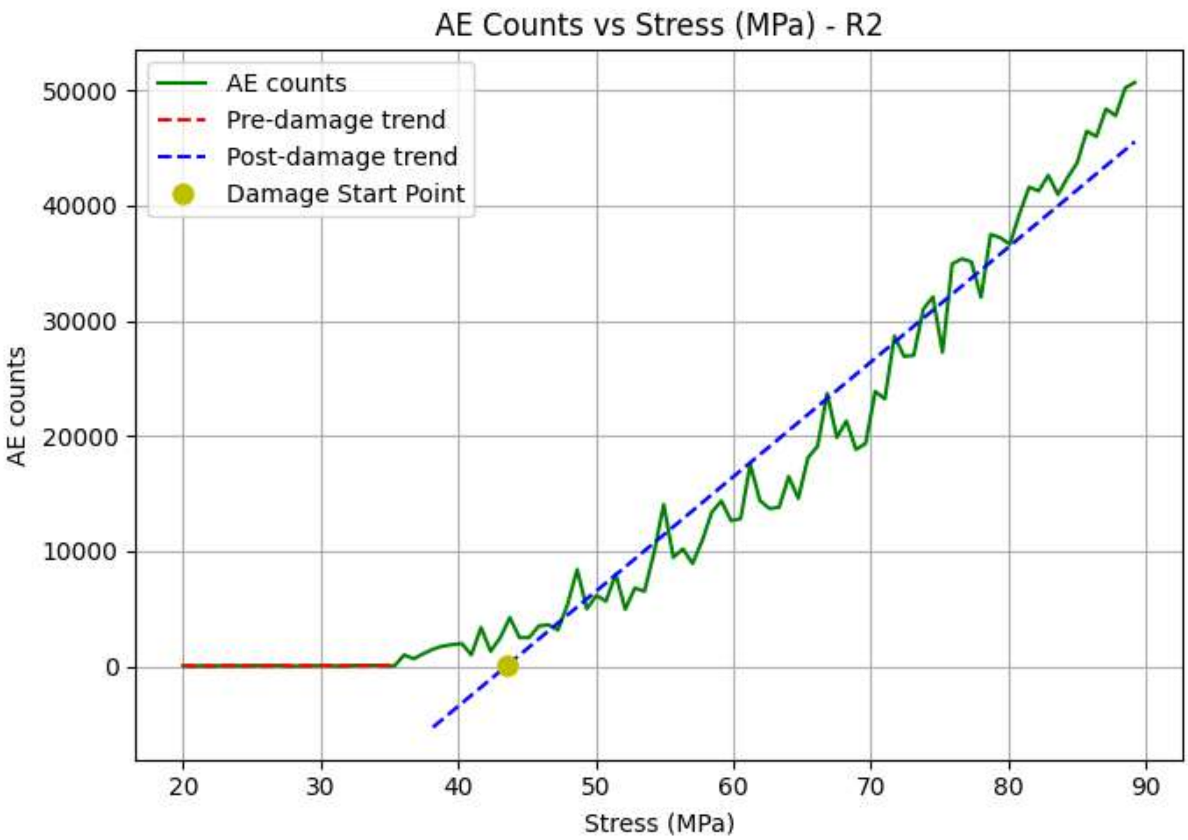

Figure 5.13 Cumulative AE counts vs UCS graph (R2)

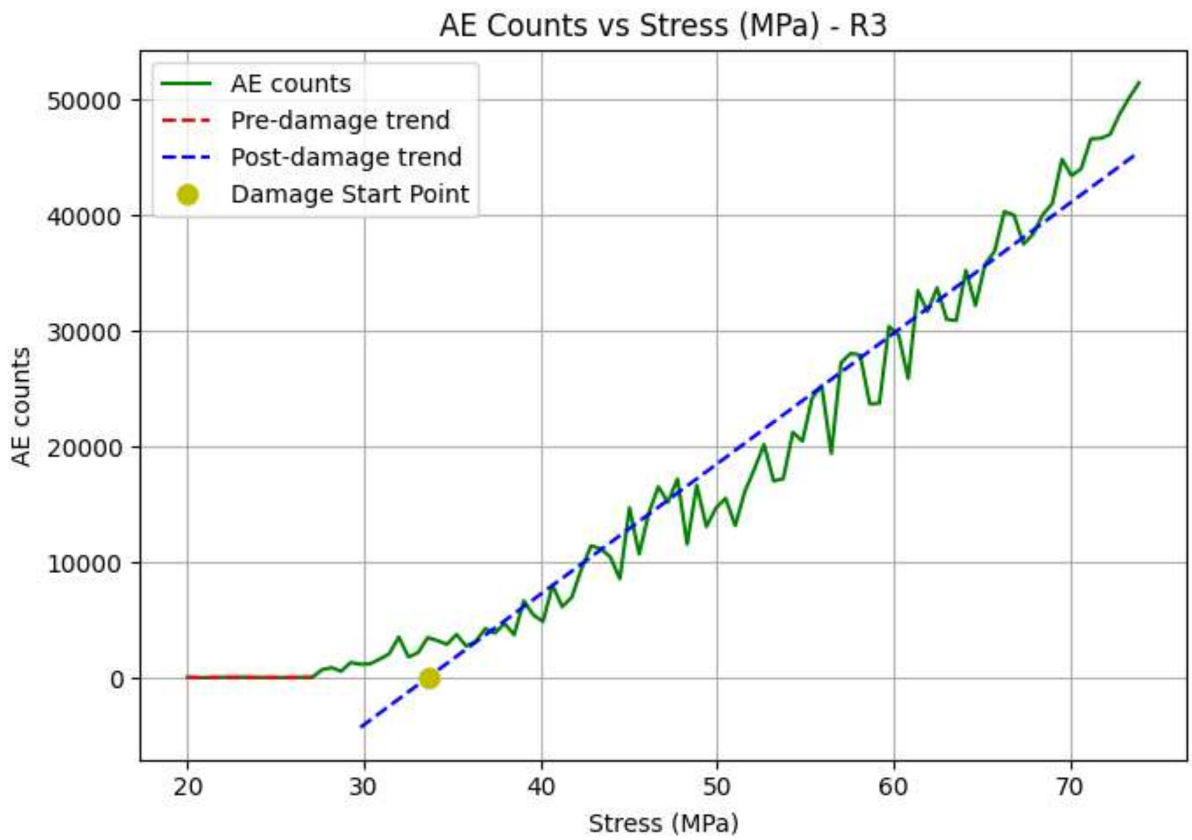

Figure 5.14 Cumulative AE counts vs UCS graph (R3)

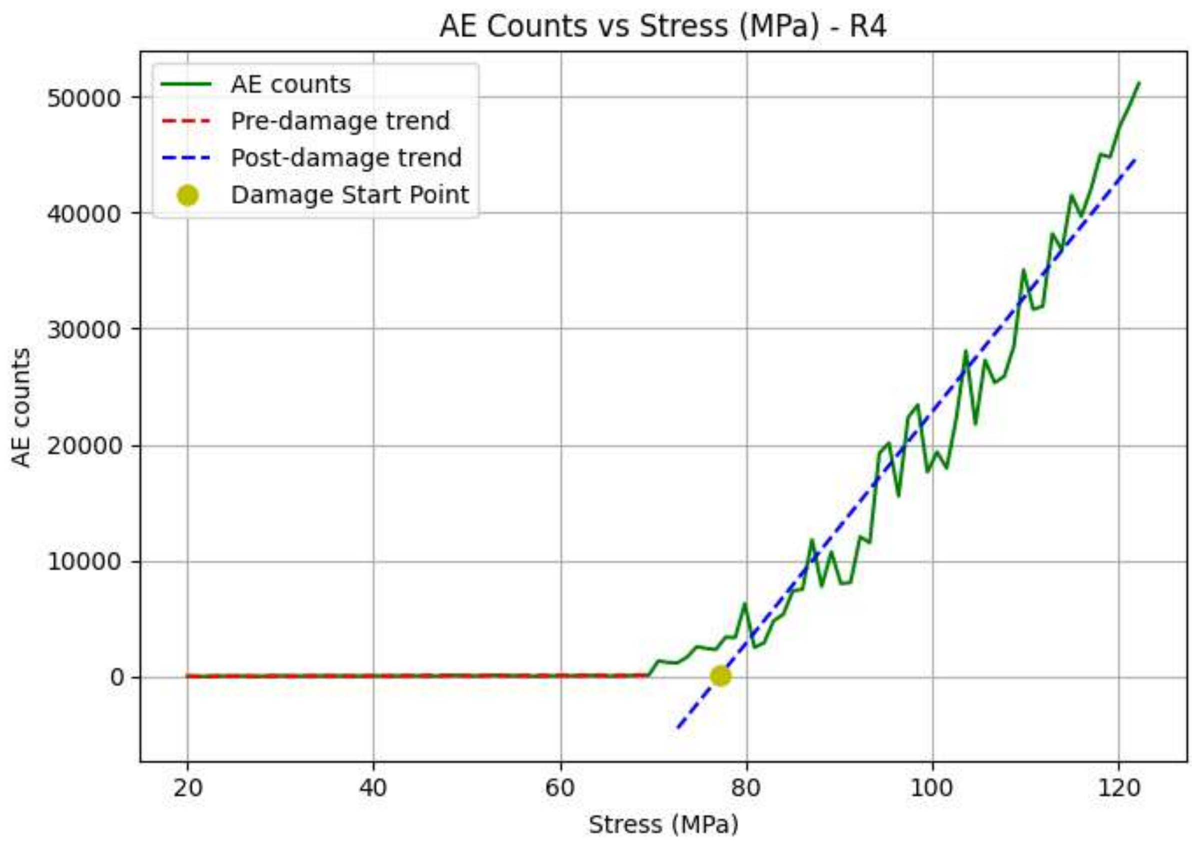

Figure 5.15 Cumulative AE counts vs UCS graph (R4)

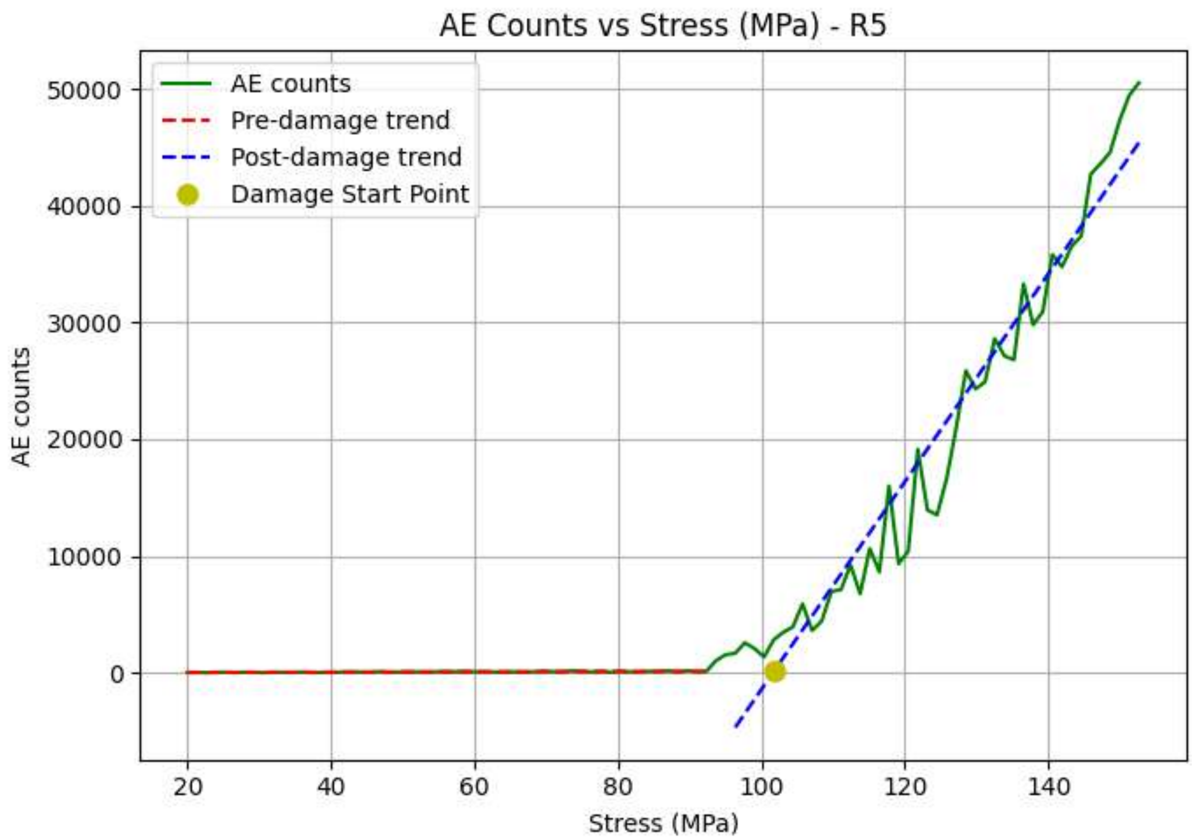

Figure 5.16 Cumulative AE counts vs UCS graph (R5)

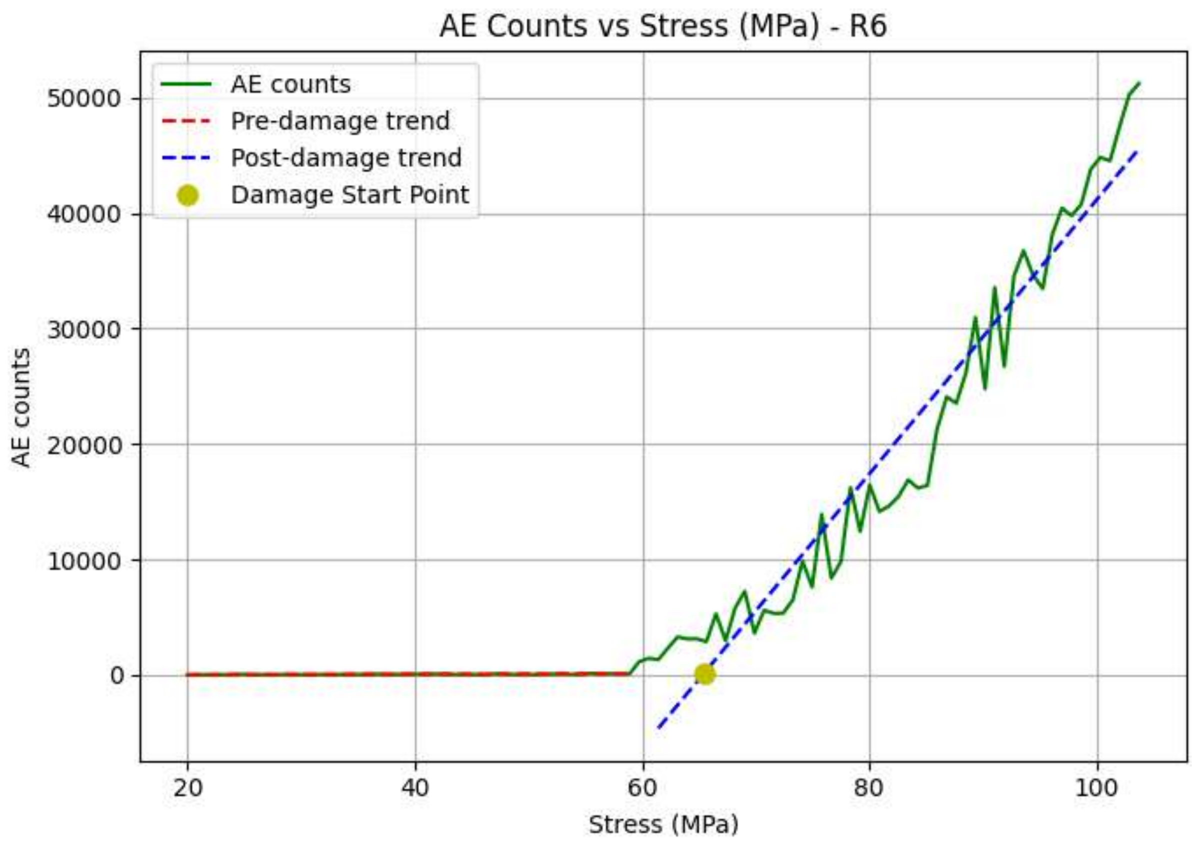

Figure 5.17 Cumulative AE counts vs UCS graph (R6)

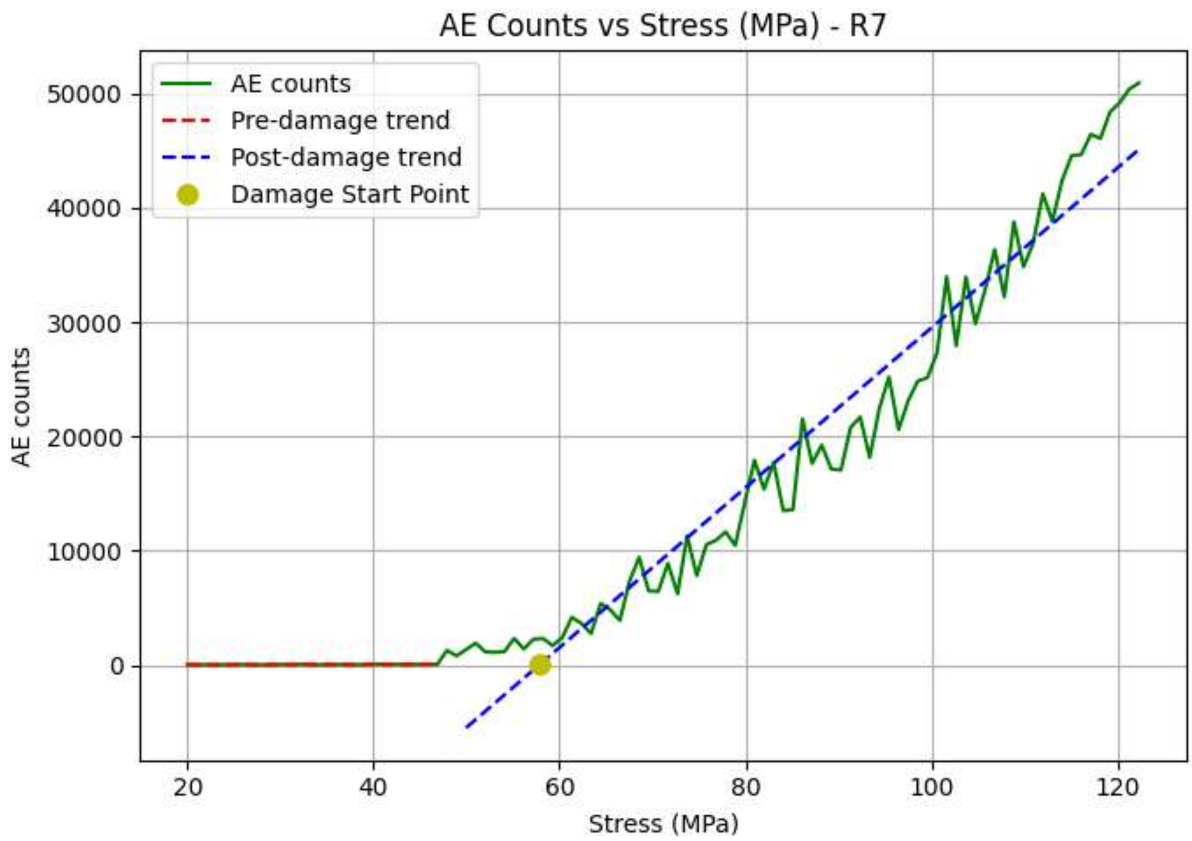

Figure 5.18 Cumulative AE counts vs UCS graph (R7)

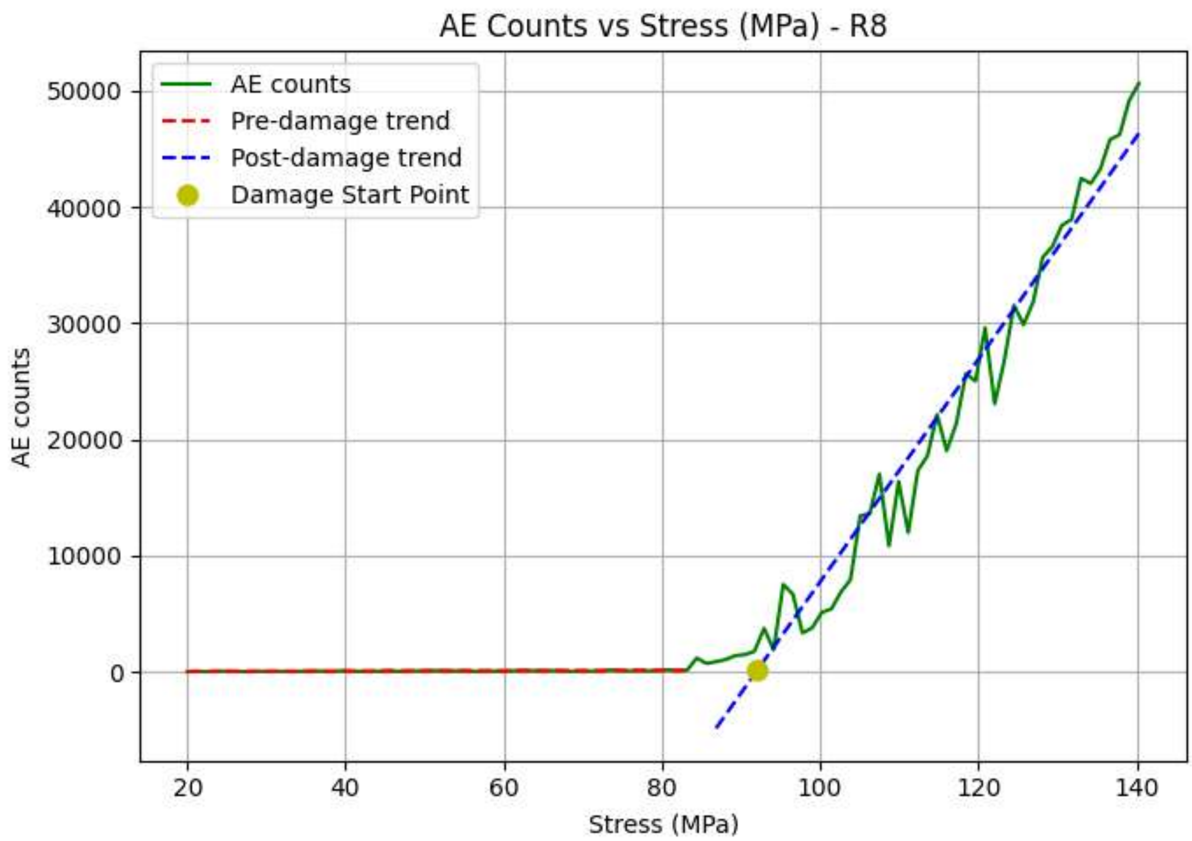

Figure 5.19 Cumulative AE counts vs UCS graph (R8)

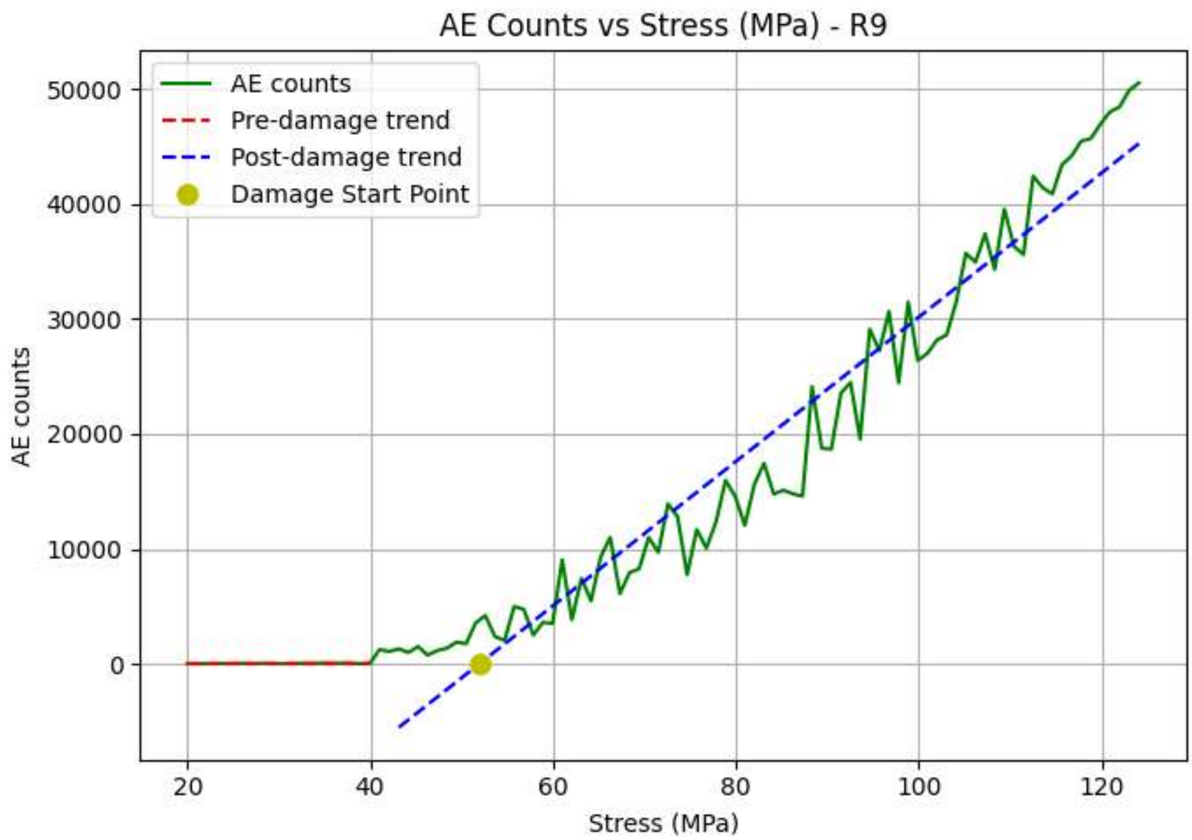

Figure 5.20 Cumulative AE counts vs UCS graph (R9)

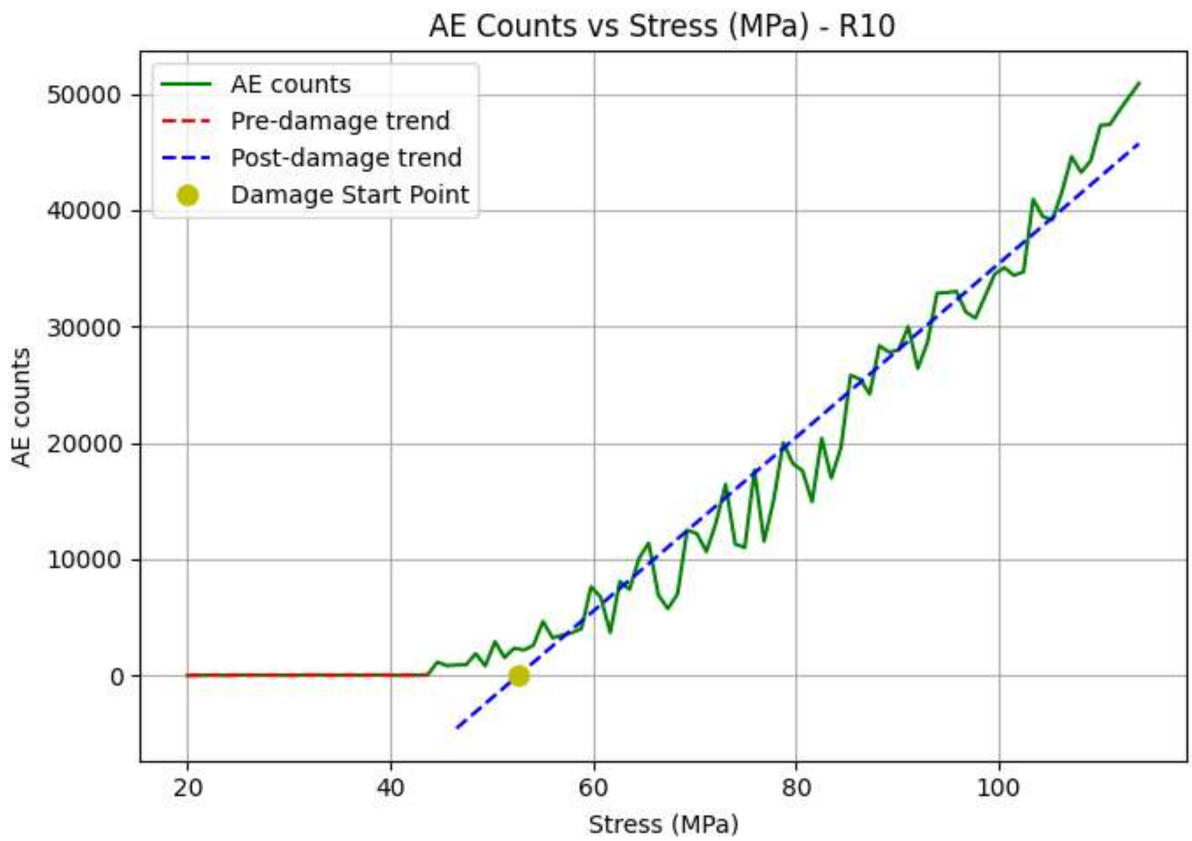

Figure 5.21 Cumulative AE counts vs UCS graph (R10)

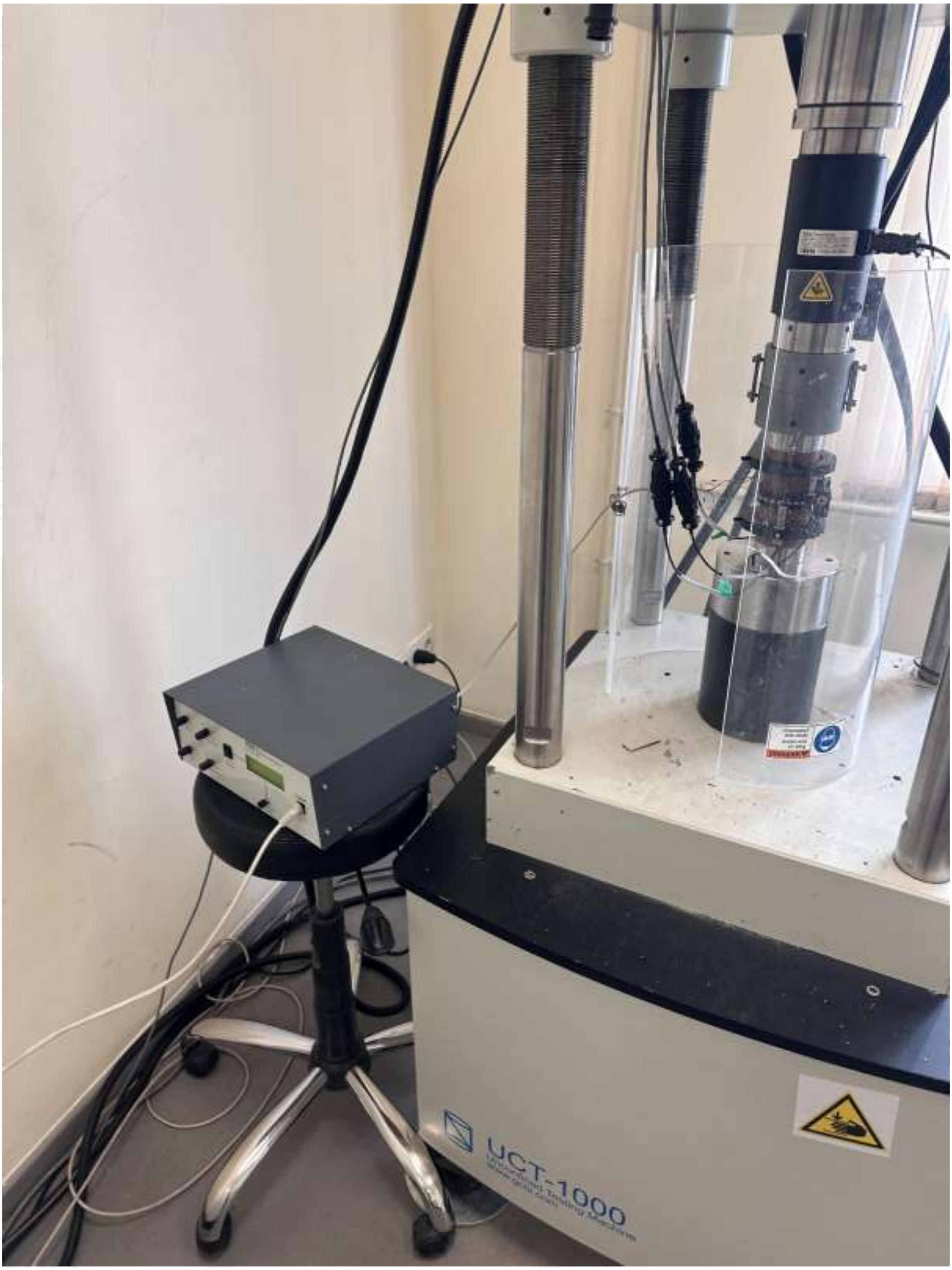
UCT-1000

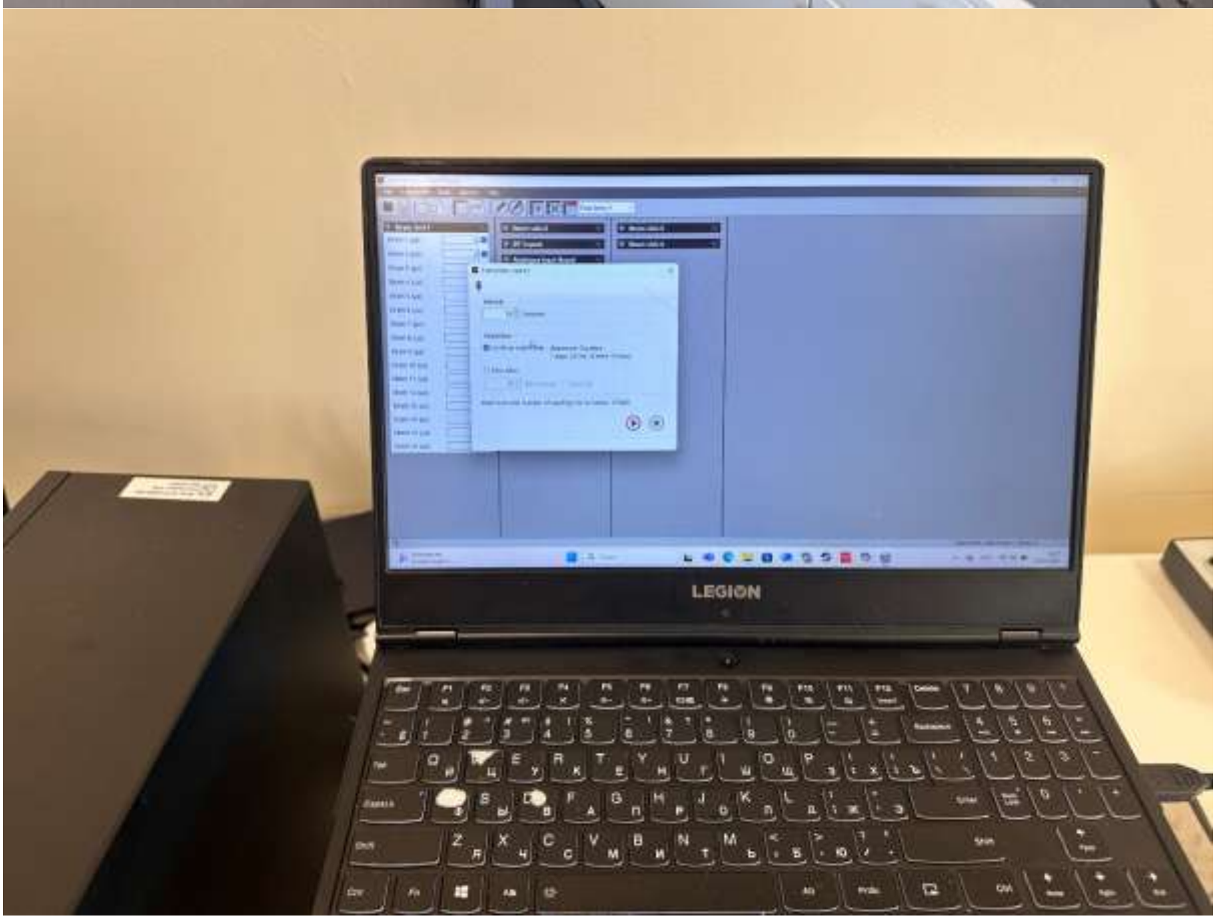
LEGION

List of symbols

a, m_b, and s - rock mass constants

σ_1 - major principal stress (MPa)

σ_3- minor principal stress (MPa)

σ_{ci} - intact rock uniaxial compressive strength (MPa)

σ_t - intact rock tensile strength (MPa)

ϕ - friction angle (°)

c - cohesive strength (MPa)

GSI - geological strength index

m_i - intact rock material constant

D - Damage factor

SL - stress level

A constant that depends on the rock mineralogical composition, texture, structure, metal content, etc.

$\mu\varepsilon$ – Strain